Spring 2023

INVESTIGATION INTO ITADORI KNOTWEED AS A CONTROL OF BANK EROSION IN NEW HAMPSHIRE RIVERS

Lauren Kaehler
University of New Hampshire, Durham

INVESTIGATION INTO ITADORI KNOTWEED AS A CONTROL OF BANK EROSION IN NEW HAMPSHIRE RIVERS

BY

LAUREN KAEHLER

B.A. Geological Sciences, University of New York at Geneseo, 2020

THESIS

Submitted to the University of New Hampshire

in Partial Fulfillment of

the Requirements for the Degree of

Master of Science

in

Hydrology

May, 2023

This thesis has been examined and approved in partial fulfillment of the requirements for the degree of Master of Science in Hydrology by:

Thesis Director, Anne Lightbody, Associate Professor of Hydrology

Michael Palace, Associate Professor of Earth Sciences

Brian Colleran, M.S Conservation Biology, CERP, PWS, AFB

On January 23, 2023

Original approval signatures are on file with the University of New Hampshire Graduate School.

ACKNOWLEDGEMENTS

Firstly, I would like to thank Anne Lightbody, for all her assistance as an advisor. I am forever grateful for all the advice you have given me throughout this process. I appreciate all the time you spent working with me in the office and the field, especially the time spent wading through freezing cold rivers in December, getting eaten alive by mosquitos in the summer, and portaging the canoe. In addition, I would like to thank Mike Palace and Brian Colleran for their enthusiasm and insight throughout this project in the world of remote sensing and Itadori knotweed.

I would also like to thank Desmond Kager, Trevor Fenoff, and Anthony Nguyen for their assistance in the field. In addition, I would like to thank Frankie Sullivan and Christina Herrick, for their assistance with all things relating to UAVs and remote sensing. Additionally, I would like to thank my parents for their endless support and help in the field with this project.

I could not have completed this project without the various sources of funding that made this project possible. I am grateful for the Dingman scholarship and grants provided by the NH Water Resource Research Center (WRRC) and the Lamprey River Advisory Committee.

Funds for this project were provided by the National Park Service under CFDA 15.962 – National Wild and Scenic Rivers System. The views and conclusions contained in this document are those of the authors and should not be interpreted as representing the opinions or policies of the U.S. Government. Mention of trade names or commercial products does not constitute their endorsement by the U.S. Government.

Table of Contents

List of Figures

List of Tables

ABSTRACT

INVESTIGATION INTO ITADORI KNOTWEED AS A CONTROL OF BANK EROSION IN NEW HAMPSHIRE RIVERS

by

Lauren Kaehler

University of New Hampshire, May, 2023

As floods increase in frequency and magnitude throughout New England, research on controls of erosion is necessary to help manage riverbank erosion and its implications on river system health and safety of infrastructure situated along the bank. *Reynoutria japonica* (Itadori knotweed) is an invasive species spreading throughout New Hampshire rivers which is suspected to cause riverbank erosion due to its unique root structure and winter die-back. To examine the impact of knotweed on riverbank erosion, paired knotweed and native species vegetation patches were selected as study sites along the Sugar and Lamprey Rivers, New Hampshire. Study sites were monitored over the course of a year using bank pins, remote sensing (LiDAR and Structure from Motion), and hydraulic modeling. Banks colonized by knotweed experienced 6.8 cm more erosion on average than similar banks with native vegetation. No statistically significant difference was recorded between modeled applied shear stress or estimated critical shear stress values between paired vegetation patches, apart from Sugar Site 6. Overall, the results of the bank erosion monitoring, estimated critical shear stress, and modeled applied shear stress results show that the only significant differences across paired vegetation patches were the presence of Itadori knotweed and an increase in erosion measured at knotweed patches. To minimize the impacts on river ecosystems by knotweed and damage to infrastructure by erosion, river corridor management should consider efforts to remove knotweed from river systems.

Chapter 1: Introduction

1.1 Importance of Studying Bank Erosion

Morphological change in river systems is controlled in part by riverbank erosion, which is a natural process dependent on many factors including regional climate, geology, soil properties, and fluvial vegetation (Lawler, 1995; Duró et al., 2019). Excessive erosion can be hazardous to aquatic ecosystems and surrounding infrastructure (Kline and Dolan, 2008). Riverbank erosion increases the amount of sediment being transported in the river, limiting the amount of light available for organisms in the river and increasing the amount of deposition downstream (Arnold and Toran, 2018). In addition, the erosion of riverbank sediment, which often contains phosphorus, has been linked to harmful algae blooms and the eutrophication of downstream lakes (Ross et al., 2019). Infrastructure such as dams, bridges, roads, and buildings located near the riverbanks are also at risk from bank erosion and can be costly to repair (Gall et al., 2011; Fluixá-Sanmartín et al., 2018; Deng et al., 2016). Therefore, erosion is a risk to public health, private property, and public infrastructure, as well as ecological functions (Deng et al., 2016).

Over the past century, flood events in New England have been increasing in frequency and severity due in part to climate change and changes in land use (Armstrong et al., 2012; Armstrong et al., 2014). More frequent extreme precipitation events have led to more large flood events (Armstrong et al., 2012; Armstrong et al., 2014; Ross et al., 2019). In addition, increased runoff due to urbanization preventing infiltration of rainwater in riparian buffers has also caused more water to reach rivers faster, causing larger floods (Ross et al., 2019). As a result of the

increase in floods, riverbanks are more susceptible to erosion than ever (Ross et al., 2019; Li et al., 2021).

Riverbank erosion is a result of a combination of multiple processes, which can vary in dominance based on geographical location, as well as location within the river system (Lawler, 1995; Chassiot et al., 2020). Processes of bank erosion include fluid entrainment, subaerial processes, and mass failure (Lawler, 1995; Chassiot et al., 2020). Fluvial entrainment happens when the force applied by water passing over the bed and bank material, known as shear stress, exceeds the stress level at which point the bank material will be mobilized, known as critical stress of the bank (Julian and Torres, 2006). In cold climates, fluvial entrainment can also be caused by the abrasion of ice against the bank (Chassiot et al., 2020). Subaerial processes, including mass failure events which are generally caused by gravitational forces along with slower "preparatory" processes such as weakening during freeze-thaw cycles, also can cause the collapse of bank material (Jugie et al., 2018). As an example, a bank could be undercut by fluvial erosion during a large flood, with the overhanging material later collapsing due to gravity in a mass failure event (Chassiot et al., 2020). The prevalence of each process depends on river and riverbank characteristics, such as discharge, channel slope, bank height, and soil cohesion (Lawler, 1995; Chassiot et al., 2020). The contribution each process makes to the total amount of riverbank erosion varies between rivers and spatially along individual rivers in part based on upstream drainage area (Lawler, 1995). Fluvial entrainment is the most dominant erosive process in the middle sections of a river (Lawler, 1995).

Bank erosion depends on fluvial processes, characteristics of bank material, and the presence of bank vegetation (Lawler, 1995; Chassiot et al., 2020). Soil properties of bank material, such as soil cohesion, grain size, moisture content, and the percentage of organic

matter, can increase or decrease critical shear strength of the bank (Lawler, 1995; Simon and Collison, 2002; Julien and Torres, 2006). Additionally, mature native vegetation has been found to stabilize riverbanks (Simon and Collison, 2002; Gurnell et al., 2016; Stover et al. 2018). Vegetation also impacts flow patterns during floods when water inundates the banks, which can influence erosion and deposition patterns (Perignon et al., 2013; Bywater-Reyes et al., 2018).

1.2 Past Research on Riverbank Erosion

Bank erosion has previously been studied using numerous different methods. In the field, erosion has been monitored in situ using cross sectional surveying and bank pins (Lawler, 1995; Heritage et al., 2009; Foucher et al., 2016; Arnold and Toran, 2018). In cross sectional surveying, repeated measurements of channel bed elevation along a cross section are compared (Heritage et al., 2009, Matte et al., 2021). Bank pins are rods installed horizontally into the riverbank (Lawler, 1993; Lawler, 1995). As the bank erodes, the amount of bank pin exposed increases, allowing quantification of the amount of erosion taking place (Lawler, 1993; Lawler, 1995). Bank pins are one of the most common methods of monitoring bank erosion (Lawler, 1993; Foucher et al., 2016; Arnold and Toran, 2018).

Remote sensing techniques such as Structure from Motion (SfM) are also increasingly used to measure bank erosion (Jugie et al., 2018; Duró et al., 2019). SfM uses hundreds of pictures taken of a surface at various angles and depths, which are entered into a computer program that is able to generate a three-dimensional model of the bank (Jugie et al., 2018; Duró et al., 2019). Photographs can be taken by hand or using an Unmanned Aerial Vehicle (UAV; Jugie et al., 2018; Duró et al., 2019). This technique can be repeated over the course of months to years to assess changes over time in the bank by comparing the 3-dimensional models (Jugie et

al., 2018; Duró et al., 2019). Due to the high spatial variability of bank erosion, SfM may be able to catch changes that bank pins could miss (Jugie et al., 2018; Chassiot et al., 2020).

Remote sensing techniques, especially those deployed via Unmanned Aerial Vehicles (UAVs), have great potential to be used to monitor riverbank erosion due to their ability to capture accurate high-quality repeated spatial data for relatively low costs (Hemmelder et al., 2018). In some cases, UAVs may be more useful than satellite imagery due to their potential higher resolution and flexibility to collect data almost anywhere or anytime (Hemmelder et al., 2018). UAVs can collect photographs necessary for SfM or can be equipped with Light Ranging and Detection (LiDAR) technology to collect topographic data (Hemmelder et al., 2018; Palace et al., 2018; Hamshaw et al., 2019). The topographic data can be used to create topographic maps, called digital elevation models (DEMs; Hamshaw et al., 2019). DEMs created from repeated flights can be subtracted from each other to create DEMs of Difference (DoDs) displaying any erosional or depositional change taking place on the banks over time (Hamshaw et al., 2019).

Hydraulic modeling is another powerful tool that has been used to quantify riverbank erosion. Numerous models have been developed to assess bank stability and sediment contribution to rivers over a range of spatial scales including the Bank Stability and Toe Erosion Model (BSTEM; Simon et al., 2003), Distributed Hydrology Soil and Vegetation Model (DHSVM; Wigmosta et al., 1994), BankforNET (Gasser et al., 2020), and the Conservation Channel Evolution and Pollutant Transport System (CONCEPTS; Langendoen, 2000). Some models, such as BSTEM, can incorporate information about bank vegetation to model the impact of root structure on bank stability through RipRoot (Stryker et al., 2017; Stover et al., 2018).

This study uses the numerical hydrodynamic model Flow and Sediment Transport with Morphological Evolution of Channels (FaSTMECH), which is offered publicly through the International River Interface Cooperative (iRIC), to model river flow (Nelson, 2013). FaSTMECH was selected as it is a quasi-steady two-dimensional model developed by the United States Geological Survey (USGS) using the continuity and Navier-Stokes equations for the conservation of fluid mass and momentum to solve for velocity and shear stress (Nelson, 2013). A two-dimensional model was selected as it can calculate applied shear stress caused by the water flowing past the bank material, which can be used to predict fluvial entrainment, and one-dimensional models do not adequately take into account river processes in meanders, which makes two-dimensional models better suited to non-straight channels (Julien and Torres, 2006; Nardi et al., 2013). The use of FaSTMECH within this study focused solely on fluvial entrainment, not other mechanisms of erosion such as mass failure and subaerial processes.

1.3 Past Research on the Impact of Vegetation on Bank Erosion

Multiple studies have investigated the impact of different types of vegetation on bank stabilization and riverbank erosion through field and flume studies. Pollen and Simon (2005) used a model and field verification of root tensile strength to determine that overall roots stabilize riverbanks, but the amount of reinforcement changed spatially and temporally based on soil shear strength and soil moisture. Gran and Poala (2001) used a flume to replicate a braided channel river and alfalfa (Medicago sativa) to simulate riparian vegetation, keeping discharge and sediment grain size constant. Vegetation stabilized the riverbanks reducing channel migration, creating narrower and deeper channels, with the effects increasing with increasing vegetation density (Gran and Poala, 2001). In a similar flume experiment, Coulthard (2005) found vegetation to increase the number of channels by acting as obstructions and directing flow

to either side, in contrast to previous studies. Though once channels were established, there was minimal later migration suspected to be caused by increased bank stability due to the vegetation (Coulthard, 2005).

Other studies have investigated the impact of vegetation on bank erosion through hydraulic modeling (Stryker et al., 2017; Bywater-Reyes et al., 2018; Stover et al., 2018). Stover et al. (2018) investigated the difference between the invasive plant *Arundo donax* (giant reed) and the native species *Salix laevigata* (red willow) on stream bank stability on the Santa Clara River in California using BSTEM. The native species was found to have both higher stem density and greater root tensile strength than the invasive, suggesting that *A. donax* provided less structural support to the riverbank (Stover et al., 2018). Bywater-Reyes et al. (2018) modeled different vegetation types and densities on point bars assessing changes in flow velocity and direction using FaSTMECH (Nelson, 2013). They found higher density vegetation had the most impact on erosional and depositional patterns within the channel compared to no vegetation and sparse vegetation (Bywater-Reyes et al., 2018).

1.4 Introduction to Itadori knotweed

The importance of bank vegetation to bank stability is highlighted when considering the spread of the invasive species Itadori knotweed (*Reynoutria japonica*), which is suspected to destabilize riverbanks (Talmage and Kiviat, 2004; Mummigatti, 2008; Secor et al. 2013; Arnold and Toran, 2018; Hammer, 2019; Matte et al., 2021). This species is also known by the common name “Japanese knotweed,” though the name “Itadori knotweed” was used throughout this study to minimize negative national associations. Itadori knotweed is a highly invasive species that has spread throughout Europe and North America from Asia (Drazan et al., 2021). Knotweed grows in dense tall clusters, which block the sun from native species, and in combination with the

potential allelopathic effects of roots, create a monoculture (Drazan et al., 2021). In addition to the harm knotweed may cause to the fluvial ecosystem, it is suspected to increase bank erosion due to its rhizomatous root structure, primarily in steep cut banks (Arnold and Toran, 2018; Colleran et al., 2020). Knotweed is also suspected to increase erosion during winter months when the plants die out and leave soil exposed to runoff or large spring-melt flood events (Child and Wade, 2000; Smets et al., 2008).

Previous studies throughout North America and Europe have investigated the potential impact of Itadori knotweed on river ecosystems. On a large scale, unmanned aerial vehicles (UAVs) and satellite imagery have been used to identify the locations of knotweed along rivers (Martin et al., 2018). Spatial and temporal spreading patterns of knotweed were projected and discussed in comparison with native species in a European river (van Oorschot et al., 2017). In modeled scenarios with both vegetative and seed dispersal, knotweed was found to outcompete native species (van Oorschot et al., 2017). Within the model, high abundance of dense knotweed patches impacted flow patterns and raised water levels during the summer, lowering sediment transport. In the winter, the die-back of knotweed left the floodplain vulnerable to erosion, increasing the amount of sediment in the river (van Oorschot et al., 2017). Other studies have focused solely on the harmful biological impact of knotweed on an ecosystem (Lavoie, 2017; Wilson et al., 2017; Fogelman et al., 2018).

Multiple field studies have investigated the correlation between knotweed and an increase in riverbank erosion. Mummigatti (2008) noted an increase in sediment load downstream of knotweed patches after rainstorms. Secor et al. (2013) found banks with knotweed lost four times the amount of soil that was lost by forested banks over a three-month study. Arnold and Toran (2018) studied the impact of knotweed on riverbank erosion through monitoring turbidity and the

use of bank pins, showing increased amounts of erosion taking place on incised banks covered with knotweed. Hammer (2019) found the percentage of riverbed embeddedness, which is a measure of the amount of fine sediment on the streambed, to be higher downstream of the invasive species, supporting past work suggesting knotweed promotes erosion of riverbanks. Matte et al. (2021) observed differences between river channel cross sections in the fall and late spring at locations with knotweed compared to those without, suggesting that knotweed increases soil erosion in riverbanks. While past studies have successfully associated knotweed with increased erosion rates, there is still uncertainty into the magnitude of the impact of knotweed on erosion and the mechanisms causing it (Colleran et al., 2020).

Because knotweed spreads primarily through the propagation of stems and rhizome fragments, there is potential for a feedback loop between knotweed and erosion (Drazan et al., 2021; Colleran et al., 2020). Within the feedback loop, the rhizome root structure of knotweed weakens riverbanks banks, which ultimately leads to bank erosion and collapse during flood events, which in turn causes the breakup of plants from the original patch and spreads fragments of stems and rhizomes, known as propagules, downstream (Colleran et al., 2020). Once the propagules are deposited on downstream banks, they grow into new patches, weakening the riverbanks in new locations and continuing the cycle (Colleran et al., 2020). The potential feedback loop emphasizes the need to better understand how bank erosion is affected by knotweed, as if left undisturbed rivers may experience more erosion as knotweed takes over fluvial ecosystems.

1.5 Research Goal

The goal of this study was to further investigate the relationship between Itadori knotweed and riverbank erosion by combining multiple known erosion monitoring methods,

including using bank pins, Structure from Motion (SfM), and hydraulic modeling using FaSTMECH. The hypothesis was that erosion rates are higher near knotweed patches than vegetation patches of native species and that fluvial entrainment, caused by applied shear stress exceeding critical shear stress, is a dominant cause of bank erosion around knotweed patches. The result of this study can help river corridor management better understand the potential impacts of Itadori knotweed on river systems and develop educated management strategies.

Chapter 2: Study Sites

2.1 Study sites

Two rivers in the state of New Hampshire were selected for this study: the Lamprey River in Rockingham County and the Sugar River in Sullivan County (Figure 1). The Lamprey River has a 553 square-kilometer drainage basin and empties into the Great Bay in Newmarket, NH (StreamStats, USGS). The Sugar River drainage basin is 715 square kilometers and empties into the Connecticut River on the border between New Hampshire and Vermont (StreamStats, USGS). The mean basin slope of the Lamprey River is 6.24% while the Sugar River has a steeper mean basin slope of 12.35% (StreamStats, USGS). The Sugar River has an active USGS gauge station in West Claremont, NH (USGS 01152500; Figure 2). The Lamprey River has an active USGS gauge station located in Durham, NH (USGS 01073500; Figure 3). The riverbed of the Lamprey River is dominantly sand and gravel and the Sugar River is mostly gravel, cobble, and boulders. The riverbank soil along the Lamprey River is dominantly Sandy loam and Loamy Sand while the Sugar River is mainly silty and sandy loams (Web Soil Survey).

The two rivers are located in similar climates with some slight differences in average temperature, precipitation, and land use. The Lamprey and Sugar River drainage basins have a mean annual temperature of 46 degrees Fahrenheit and 44 degrees Fahrenheit, respectively (StreamStats, USGS). The Lamprey River drainage basin receives an average of 45 inches of precipitation annually, including 66 inches of snowfall (StreamStats, USGS). The Sugar River receives 39 inches of precipitation on average annually, including 78 inches of snowfall (StreamStats, USGS). The Lamprey River drainage basin has 9.97% of land classified as urban, 19.19% coniferous forest, 31.11% mixed coniferous and deciduous forest, and 8.59% wetlands (StreamStats, USGS). The Sugar River drainage basin is made up of 7.49% urban land, 26.93% coniferous forest, 24.66% mixed coniferous and deciduous forest, and 7.12% wetlands (StreamStats, USGS).

Based on preliminary reconnaissance of portions of the Lamprey and Sugar Rivers in the spring of 2021, a total of seven study sites were selected for this study (Figure 2; Figure 3; Figure 4). Three study sites (Sugar Site 2, Sugar Site 6, and the Lamprey Site) were selected for focal analysis using bank pins, SfM, and modeling (Figure 5). Four study sites (Sugar Site 1, Sugar Site 3, Sugar Site 4, and Sugar Site 5) were less intensively analyzed using bank pins only (Figure 6). Each study site contained two bank vegetation patches that were comparable in terms of observed flow patterns, bank height, material, and steepness; one of the bank vegetation patches was *Reynoutria japonica* (Itadori knotweed) and the other was native vegetation.

2.2 Hydrographic Analysis of Study Rivers

Discharge in both rivers was monitored by USGS during the study period, which lasted from August 2021 to October 2022. Discharge was higher than seasonal average levels from July 2021 to September 2021. Discharge continued to remain at average or higher than average levels

until March 2022. As a result of statewide drought conditions, April 2022 to October 2022 had average to below average flows. Within the study period, discharge was highest between the months of October 2021 and April 2022 (Figure 7). Discharge was lowest between June 2022 and September 2022, when daily discharge was frequently below normal for both rivers (Figure 7). The highest flow recorded in the hydrograph (Figure 7) happened in July 2021 before bank pins were installed within the study rivers, but the highest flow recorded during the study period took place in February 2022.

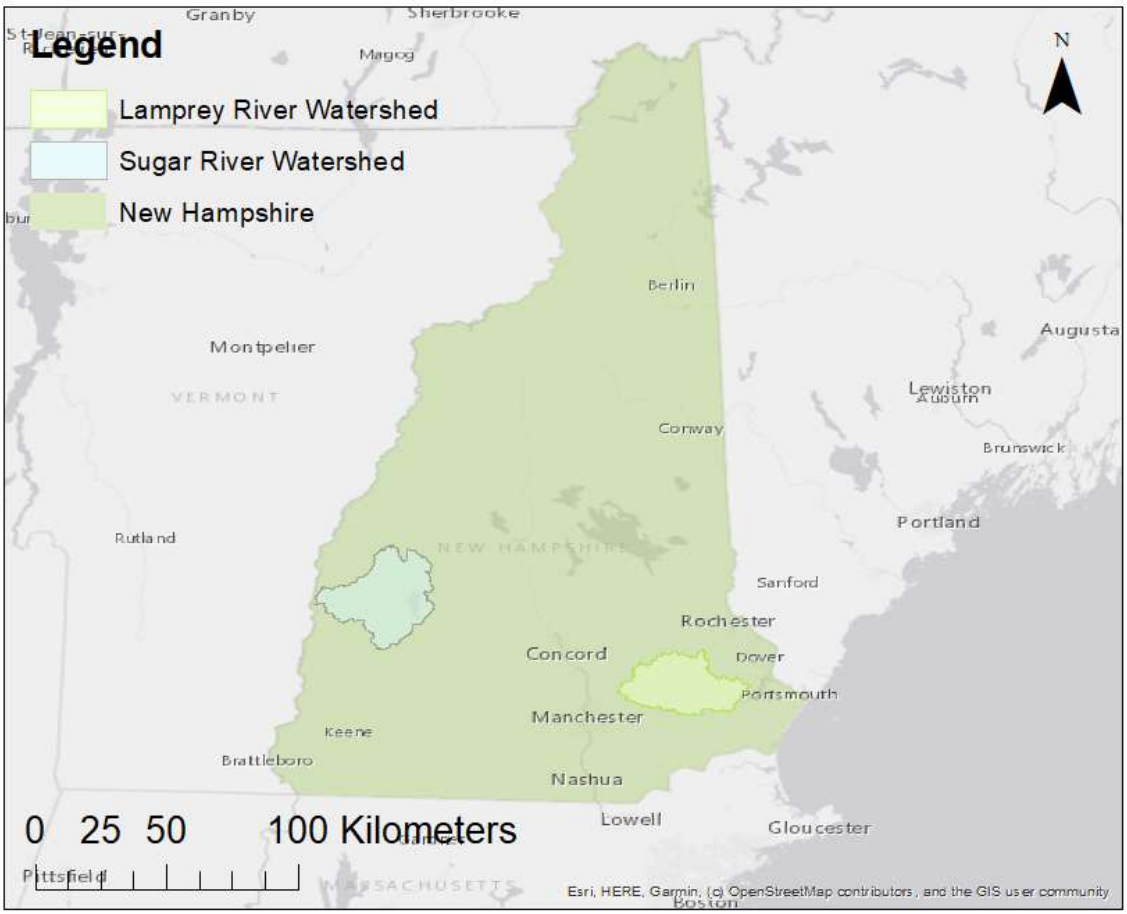

Figure 1. Locations of the Lamprey River and Sugar River watersheds within New Hampshire.

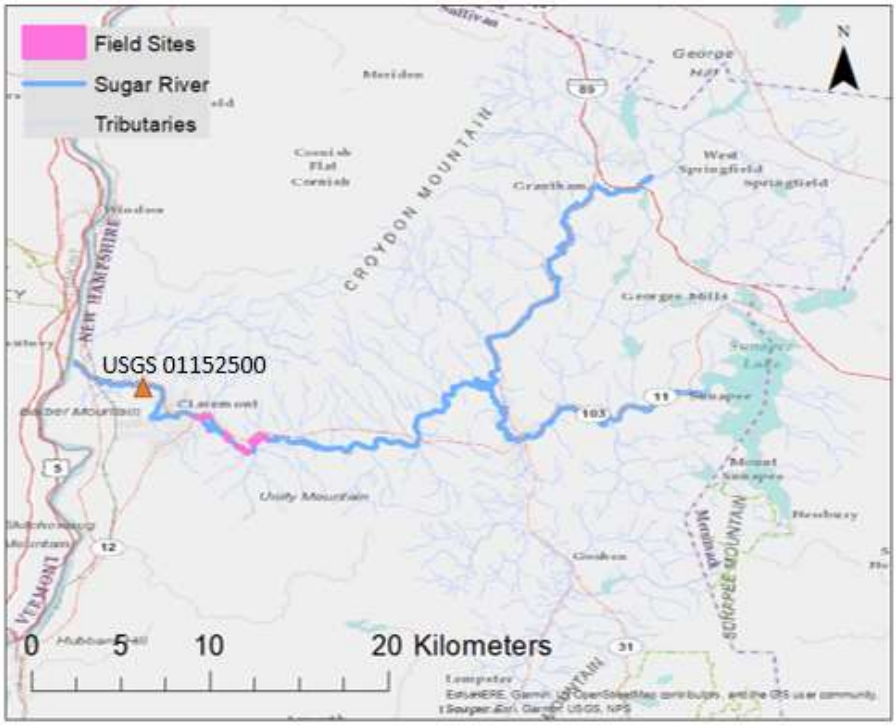

Figure 2. Locations of the six study sites on the Sugar River, which flows from east to west. The sites are in numerical order from upstream to downstream, and the gauging station is marked by an orange triangle.

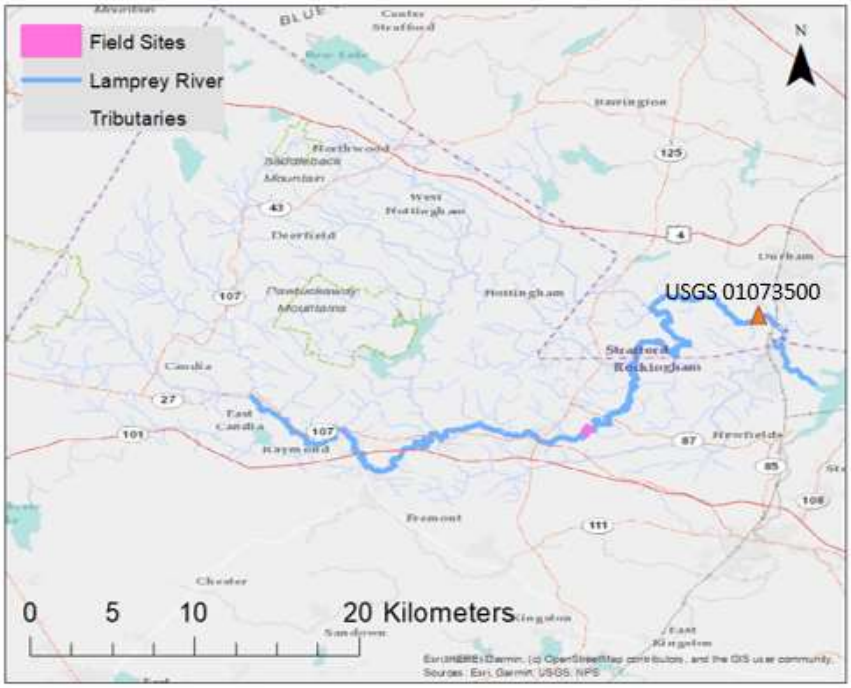

Figure 3. Location of the Lamprey Site along the Lamprey River, which flows from west to east. The gauging station is marked by an orange triangle.

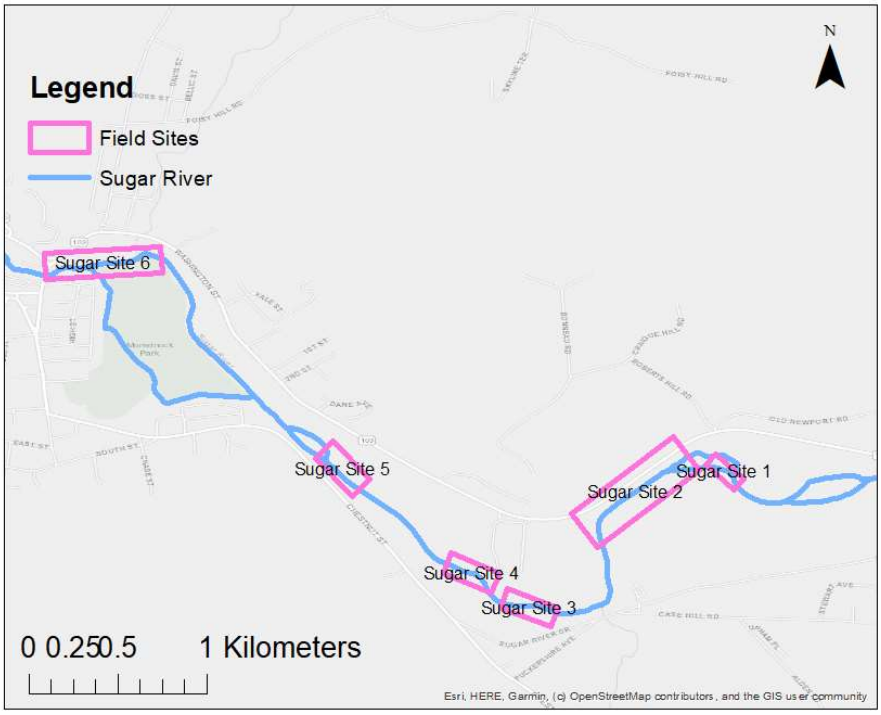

Figure 4. Locations of the six study sites on the Sugar River, which flows from east to west.

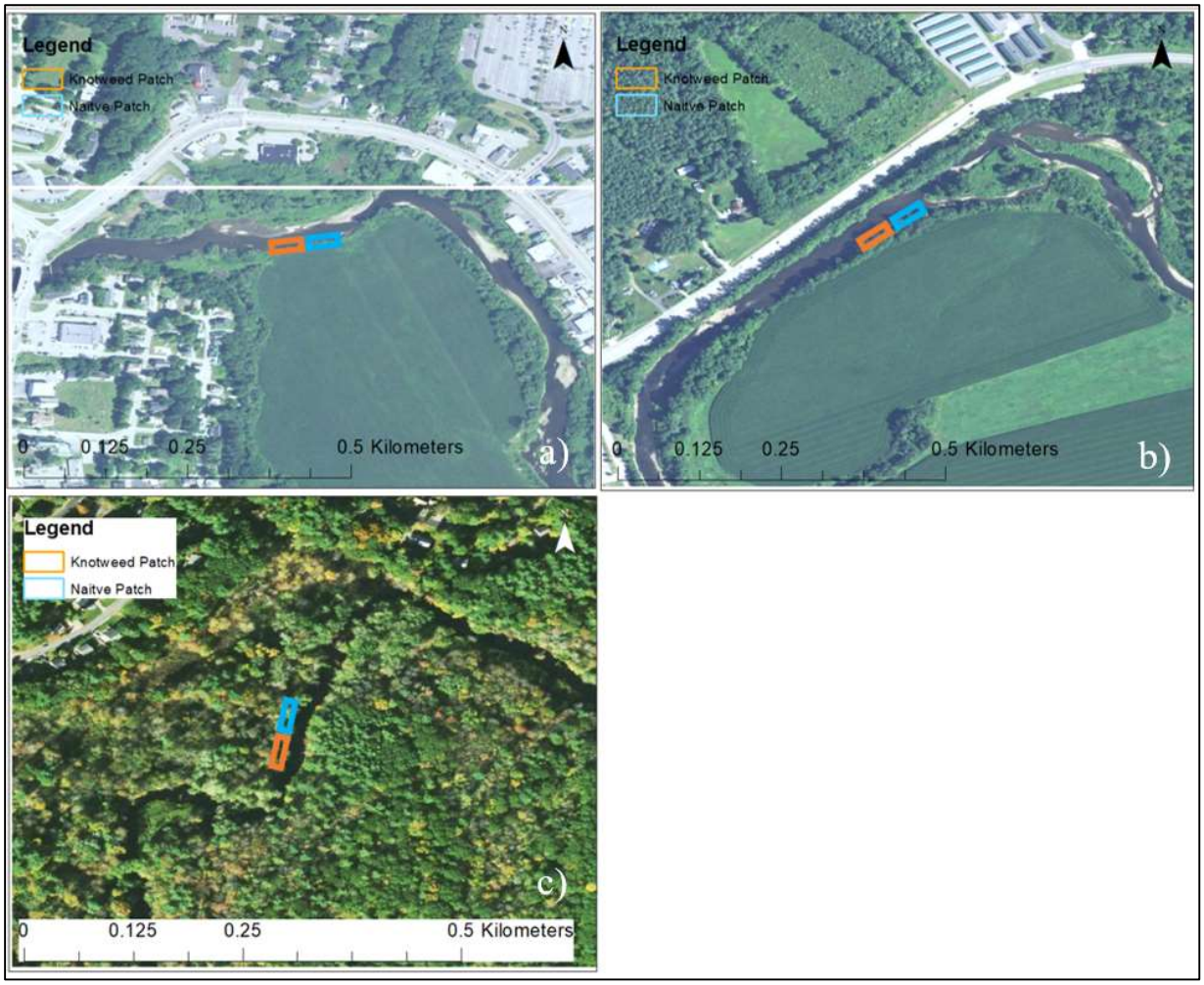

Figure 5. Aerial leaf-on imagery of the focal study sites, a) Sugar Site 2, b) Sugar Site 6, and c) Lamprey Site. Direction of flow is right to left in a) and b) and left to right in c).

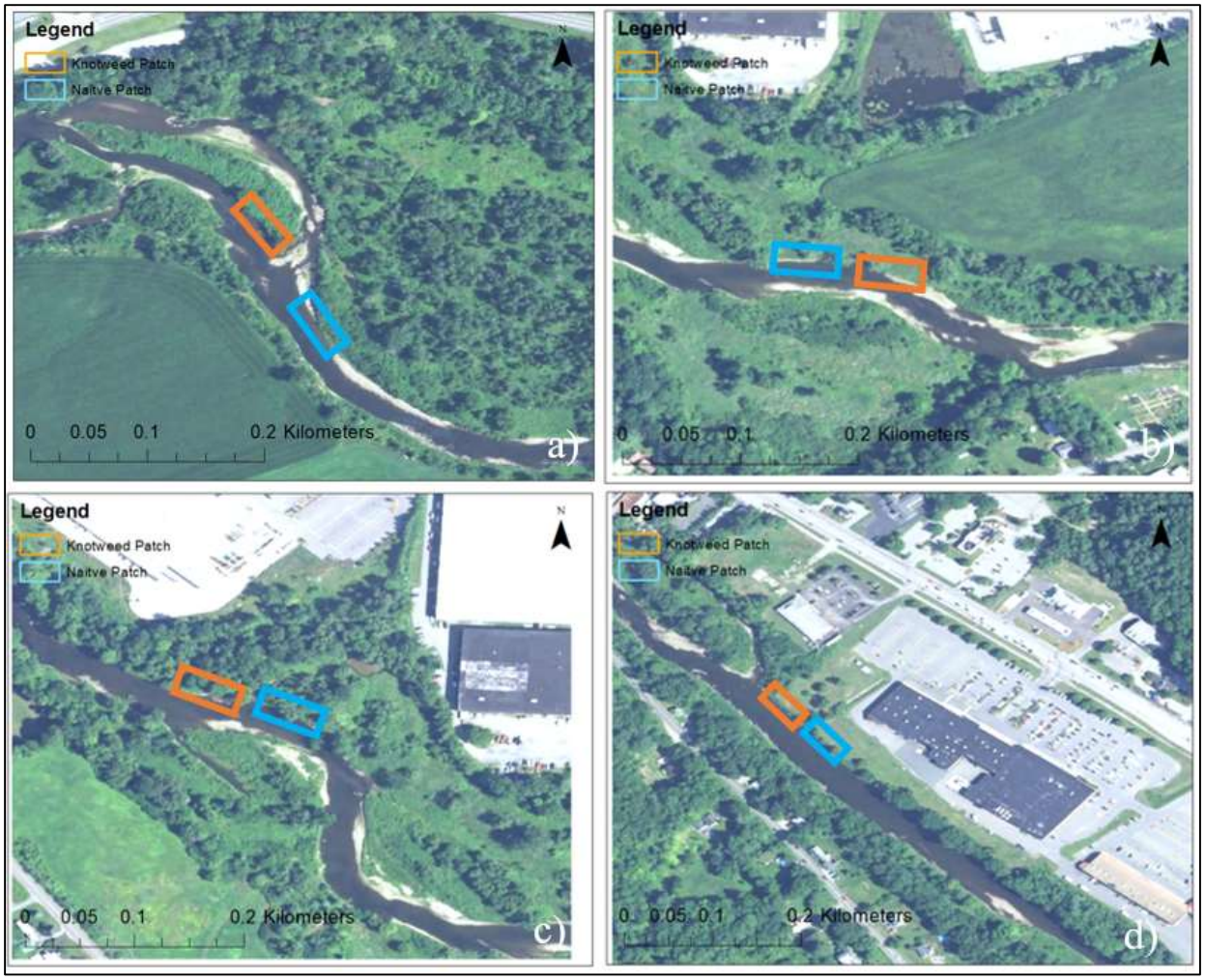

Figure 6. Aerial leaf-on imagery of the non-focal study sites, a) Sugar Site 1, b) Sugar Site 3, c) Sugar Site 4, and d) Sugar Site 5. Direction of flow is right to left.

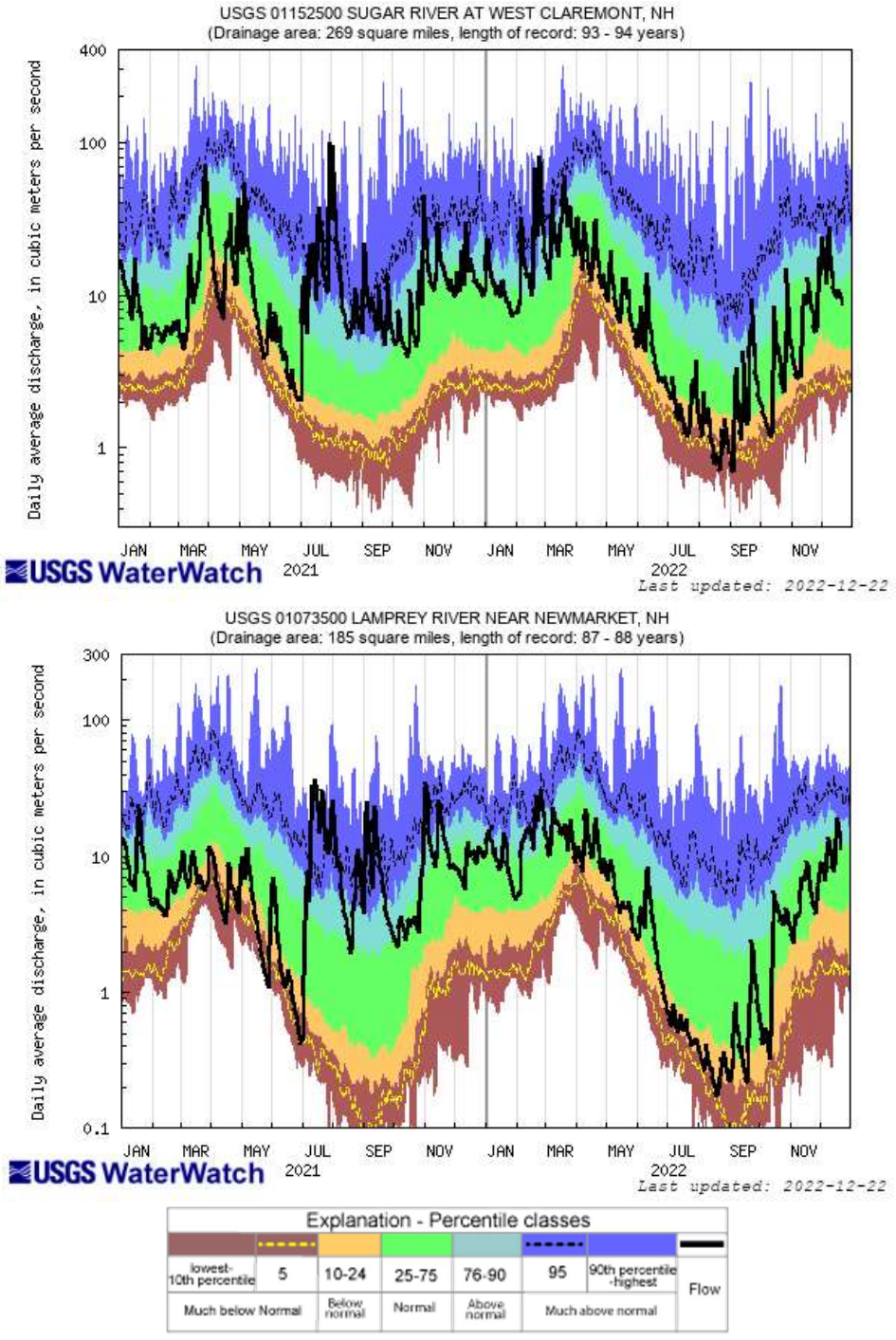

Figure 7. Hydrographs for the Sugar and Lamprey Rivers (USGS WaterWatch). The black lines indicate the daily average discharge throughout the study period, while colored lines represent historical average daily discharge levels.

Chapter 3: Methods

3.1 Knotweed Survey

Portions of the Lamprey River and Sugar River were surveyed for locations of *Reynoutria japonica* (Itadori knotweed) in the Spring and Summer of 2021 and Summer of 2022. The location of each knotweed patch was recorded, along with visual estimations of patch length, patch width, bank material, bank slope, and bank height for each patch. Future surveys on these rivers may be used to monitor the spread of knotweed throughout each river by comparison to the results of the 2021 baseline survey.

3.2 Erosion Monitoring

3.2.1 Erosion Monitoring with Bank Pins

Twelve bank pins were installed at each of the seven study sites (six on the Sugar River and one on the Lamprey River) in order to monitor the amount of erosion taking place at those locations. Each bank pin consisted of a 2-foot (61 cm) long ¼" inch (0.64 cm) diameter steel piece of rebar. A sledgehammer was used to pound each bank pin horizontally into the face of the riverbank until refusal, with a minimum of 5 cm of pin left exposed (Lawler, 1993). Two-foot-long pins were selected in this study due to the expected amount of erosion, cost, and ease of use (Lawler, 1993). Some past studies have used longer pins to prevent pins from being lost due to large amounts of erosion (Lawler, 1993; Jugie et al., 2018).

The pins were installed in vertical columns, each consisting of a top, middle, and bottom pin. The three pins were placed vertically at equal distances from each other, with the bottom pin placed just above the water surface on the day of installation, and the top pin placed at

approximately two-thirds of the total exposed bank height (Jugie et al., 2018). Within each of the knotweed patch and native species patch, two columns of pins were installed one meter apart from each other (Jugie et al., 2018). Bank pins, including those used in a similar arrangement to this study, are a well-established method to monitor riverbank erosion (Foucher et al., 2016; Jugie et al., 2018). Three bank pins have been shown to account for vertical spatial variability in bank erosion, and two columns have been used to assess lateral spatial variability in bank erosion (Jugie et al., 2018; Chassiot et al., 2020).

Bank pins were installed during August and September 2021. The bank pins at the Lamprey River site were installed on August 11th, 2021, the bank pins at Sugar River Site 6 were installed on August 18th, 2021, and bank pins were installed at all other sites on September 23rd, 2021. Bank pins were removed on September 29th, 2022 for all Sugar River sites and October 2nd, 2022 for the Lamprey River site. Bank pins at the focal sites (Lamprey, Sugar Site 2, and Sugar Site 6) were measured between three and four times after installation to assess how erosion rates varied temporally throughout the year. Bank pins at the other sites were only measured during installation and removal.

Large amounts of erosion were observed at some of the focal sites, which were each visited multiple times. In some cases, more than half of a bank pin had been exposed by erosion between visits, at which point the pin was reset to prevent the pin from falling out of the bank. At Sugar Site 2, all the knotweed bank pins except for the upstream top pin and the middle downstream native pin were reset on April 19th, 2022. At Sugar Site 6, one of the native vegetation pins had to be reset during a site visit on September 23rd, 2021, and all pins except the upstream bottom knotweed pin were reset during a site visit on April 29th, 2022.

The same procedure for measuring bank pins was used at all study sites. For each pin, the amount of pin exposed extending horizontally away from the bank soil surface was measured using a measuring tape along the top and bottom of each pin, and the average of those two values was used in the analysis (Lawler, 1993). For all study sites, the total amount of erosion taking place was determined by subtracting the final pin measurement taken the day of pin removal from the original measurement taken the day of pin installation; thus, a negative change indicated erosion. For focal study sites, the amount of erosion between successive visits was also calculated using the same process but subtracting the measurement from the later visit from that of the earlier visit.

There are various methods of interpreting bank pin results, specifically when there are positive values, as they can be caused by several factors, including deposition, bank pin movement, bank expansion and contraction, freeze-thaw, and desiccation (Lawler, 1993; Couper et al., 2002). In this study, positive values of bank pin exposure were included in the analysis as representing deposition, which is one of the standard methods of accounting for positive bank pin change (Lawler, 1993; Couper et al., 2002).

Missing bank pins pose a problem in interpreting study results. For accurate results when using bank pins, they must not move throughout the study (Lawler, 1993). Past studies have used different methods when interpreting results with missing bank pins, including assigning a bank pin change value to the pin as the maximum amount of erosion before a pin would likely fall out of the bank (Lawler, 1993). In this study, it was assumed that all the missing bank pins were lost due to mass failure of the bank, burial, or ice jams, not fluvial entrainment to a depth which would cause the bank pins to fall out of the bank. As a result, two methods were used in this analysis. In one method, unrecovered bank pins were omitted from the analysis of total bank

erosion (all sites) as well as the short-term erosion between successive visits (focal sites only). In the other method, any sites that had unrecovered bank pins (Sugar Site 3, Sugar Site 5, and Sugar Site 6) were removed entirely from the analysis. Using these methods results in a conservative estimate of erosion.

Statistical tests were used to determine if there was a significant difference in average erosion between knotweed and native vegetation patches. First, a t-test was used to compare bank pin results between knotweed and native vegetation patches. The t-test was run twice. One test included data from all sites apart from any missing bank pins. The second test only used data from Sugar Site 1, Sugar Site 2, Sugar Site 4, and the Lamprey Site. T-tests were conducted at a significance level of 0.05 and were run in python 3.8 using the SciPy Stats package. In addition, seasonal changes in erosion rates were compared using a two-way ANOVA test including interactions at a significance level of 0.05 conducted in Microsoft excel.

3.2.2 Erosion Monitoring using Structure from Motion

In addition to bank pins, focal study patches were monitored using Structure from Motion (SfM) from the ground. Hundreds of overlapping photographs were taken using an OLYMPUS Tough TG-6 Waterproof Camera on multiple dates throughout the study period (Table 1). Photographs were taken at various distances, heights, and angles relative to the bank at each vegetation patch of the three focal study sites (Jugie et al., 2018). These photographs were patched together using pix4D to generate a dense three-dimensional point cloud (Jugie et al., 2018). Point clouds were georeferenced using the outer end of each of the bank pins, which were surveyed in the field using a Trimble Geo7X Centimeter edition with Tornado 2 Antenna and Trimble TerraSync 5 software.

Table 1. Dates photographs were taken of each focal site for SfM.

Site Name	8/11/2021	8/18/2021	10/14/2021	12/10/2021	4/29/2022	9/29/2022	10/2/2022
Sugar Site 2			X	X	X	X	
Sugar Site 6		X		X	X	X	
Lamprey Site	X			X	X		X

3.3 Site-specific Vegetation Surveying

During Summer 2021, a vegetation survey was conducted at each study site. At all three focal study sites (Lamprey Site 1, Sugar Site 2, and Sugar Site 6), an in-depth survey was completed at three one-square-meter quadrats for each patch. The middle quadrat was located above the center of the bank pins installed in the patch; the two other quadrats were located one meter upstream and downstream of the middle quadrat. Within each quadrat, all vegetation that was over knee height (about 0.5 meters) was identified, and the number of stems was counted. At the non-focal study sites (Sugar Site 1, Sugar Site 3, Sugar Site 4, and Sugar Site 5), vegetation of each patch was visually classified as dense or sparse and the dominant vegetation type, such as knotweed, herbaceous, or shrub-sapling, was noted. The Shannon diversity index was used to quantify species diversity within each vegetation patch (Shannon, 1948). A Student's t-test was used to determine any significant differences in diversity between the sites.

3.4 Hydraulic Modeling of Erosion Susceptibility

The numerical hydraulic model FaSTMECH (Nelson, 2013) was used at the three focal study sites (Lamprey, Sugar Site 2, and Sugar Site 6) to provide a detailed spatial analysis of flow patterns and shear stress to understand erosion susceptibility. Similar studies have been conducted by Julian and Torres (2006), Rinaldi et al. (2008), and Bywater-Reyes (2018).

3.4.1 Acquisition of Topographic Data Using LiDAR

To accurately model the study sites, topographic data were acquired using remote sensing techniques. Topographic data of the floodplain and banks were acquired with Unmanned Aerial Vehicles (UAVs) on August 15th, 2022, for the Sugar River sites and August 24th, 2022, for the Lamprey Site. A DJI M300 drone equipped with a Livox Avia LiDAR sensor integrated into a GreenValley LiAirV70 payload was used. Flights were conducted at a flight speed of 5 m/s and an elevation of 65 m from the ground with a targeted overlap of around 60%. Data were georeferenced in LiGeoreference (v 1.4, GreenValley International, Ltd. 2022) using a NovAtel EG320N INS paired with a NovAtel base station for post-processing kinematic georeferencing of LiDAR returns. Flight lines were subsequently trimmed to produce an overlap of approximately 50%, with automated outlier removal, followed by ground classification using Lidar360 (v 5.4, GreenValley International, Ltd. 2022). The resulting total return density was greater than 300 points per square meter.

3.4.2 Acquisition of Topographic Data Using Photogrammetry

In addition to LiDAR, a DJI P4 Multispectral drone was flown over each focal site in order to collect aerial imagery for SfM (Table 2). Flight altitude was set at 100 m above the ground surface for all flights. This elevation was selected as low enough to produce high-quality imagery while being high enough to minimize flight time and the risk of hitting trees or powerlines. In this study, 60% side and 80% front overlap of photographs were used in order to minimize spatial uncertainty and create an accurate DEM (Clapuyt et al., 2016; Hemmelder et al., 2018). The flights were flown during the spring to minimize vegetation cover and take place after snow cover had melted. The aerial images were used to create a point cloud using

Pix4Dmapper. The point cloud was used to make a Digital Elevation Model (DEM) of each of the focal sites in ArcMap 10.8.1.

Table 2. Information about SfM UAV flights.

Site	Flight Date	Area Covered (km^2)	Number of Photographs	Number of Points in Point Cloud	Point Density (points per m^3)
Sugar Site 2	4/2/2022	0.346	958	8805925	22.3
Sugar Site 2	9/16/2022	0.458	5670	65761585	20.54
Sugar Site 6	4/2/2022	0.16	382	3841163	22.3
Sugar Site 6	9/16/2022	0.397	2500	7765957	7.14
Lamprey Site	5/5/2022	0.752	1129	29801064	20.1
Lamprey Site	9/16/2022	1.1	3252	33373673	20.42

The point clouds acquired through SfM were interpolated using the Inverse Distance Weighted (IDW) spatial analyst tool in ArcMap 10.8.1 to create a visual DEM. The DEMs of each focal site created using SfM were used when developing the hydraulic model, discussed later, before LiDAR data were acquired. The aerial images of the focal sites could also be used in the future to further develop methods to identify knotweed through remote sensing, which could prove useful for river corridor management groups (Martin et al., 2018).

3.4.3 Acquisition of Bathymetric Data Using Surveying

Subaqueous bathymetry of the river channels was obtained from ground surveying. Eye-safe LiDAR signals are absorbed and refracted differently by the water in a way that either prevents returns or makes them highly inaccurate (Bangen et al., 2014), so LiDAR data were not available for areas that were covered by water at the time of surveying. More specifically, bathymetric points were obtained using a Trimble Geo7X Centimeter edition with Tornado 2 Antenna and Trimble TerraSync 5 software. Survey points were obtained along cross sections

throughout the study reach, except for topographically complex regions of the channel bed or areas with large changes in slope where additional points were obtained (Heritage et al., 2009, Bangon et al. 2014). Point densities resulting from the ground survey were 0.001 point/m^2, 0.027 point/m^2, and 0.116 point/m^2 for Sugar Site 2, Sugar Site 6, and the Lamprey Site, respectively.

3.4.4 Comparison of LiDAR and SfM

Digital Elevation Models (DEMs) were created from the LiDAR and SfM data. To assess the accuracy of the resulting DEMs, the vertical alignment of the ground survey points and the LiDAR and SfM DEMs were compared. For the LiDAR data, Sugar Site 2, Sugar Site 6, and the Lamprey Site had average differences between the LiDAR and ground surveying points of 0.17 m (SD = 0.57 m, N = 10), -0.16 m (SD = 0.37 m, N = 11), and 0.23 m (SD = 0.56 m, N = 12), respectively. For the SfM data, Sugar Site 2, Sugar Site 6, and the Lamprey Site had an average difference of 0.29 m (SD = 0.34 m, N = 10), 0.24 m (SD = 0.51 m, N = 11), and - 0.43 m (SD = 0.56 m, N = 12), respectively. LiDAR had an average difference in elevation of 18.7 cm in from the ground survey points, while SfM had an average difference of 31.7 cm compared to the ground survey points. In this study, the LiDAR DEM was selected over the SfM data to be used in the hydraulic model as it was more accurate compared to the survey data. But depending on the resolution requirements of a study, SfM may be more cost effective than LiDAR.

3.4.6 Creating Digital Elevation Models

The first step to creating DEMs for the study sites was processing the ground survey data. First, individual survey points with high vertical or horizontal error were removed based on error calculations by the GPS device. Eleven points were removed from Sugar Site 2, eight points were removed from Sugar Site 6, and fourteen points were removed from the Lamprey Site;

usually these points were located near a riverbank underneath dense tree canopy. Second, additional estimated supplemental points were added in areas that were unable to be surveyed, for example in areas that were too deep to access safely. Survey points were also added far upstream and downstream of the study vegetation patches, where time constraints and deep water limited surveying, to allow the flow conditions in the hydraulic model to stabilize before reaching the vegetation patches. Around 20 to 100 points were added to each site, primarily far upstream and downstream of the vegetation patches.

After necessary corrections to the survey points were made, a riverbed surface was interpolated from the points using the Inverse Distance Weighted (IDW) spatial analyst tool and merged with the LiDAR DEMs in ArcMap 10.8.1 using the Mosaic to New Raster tool (Figure 8). The new merged DEM, with both topographic and bathymetric data, was converted to text file format using the Spatial Analyst Sample tool and exported.

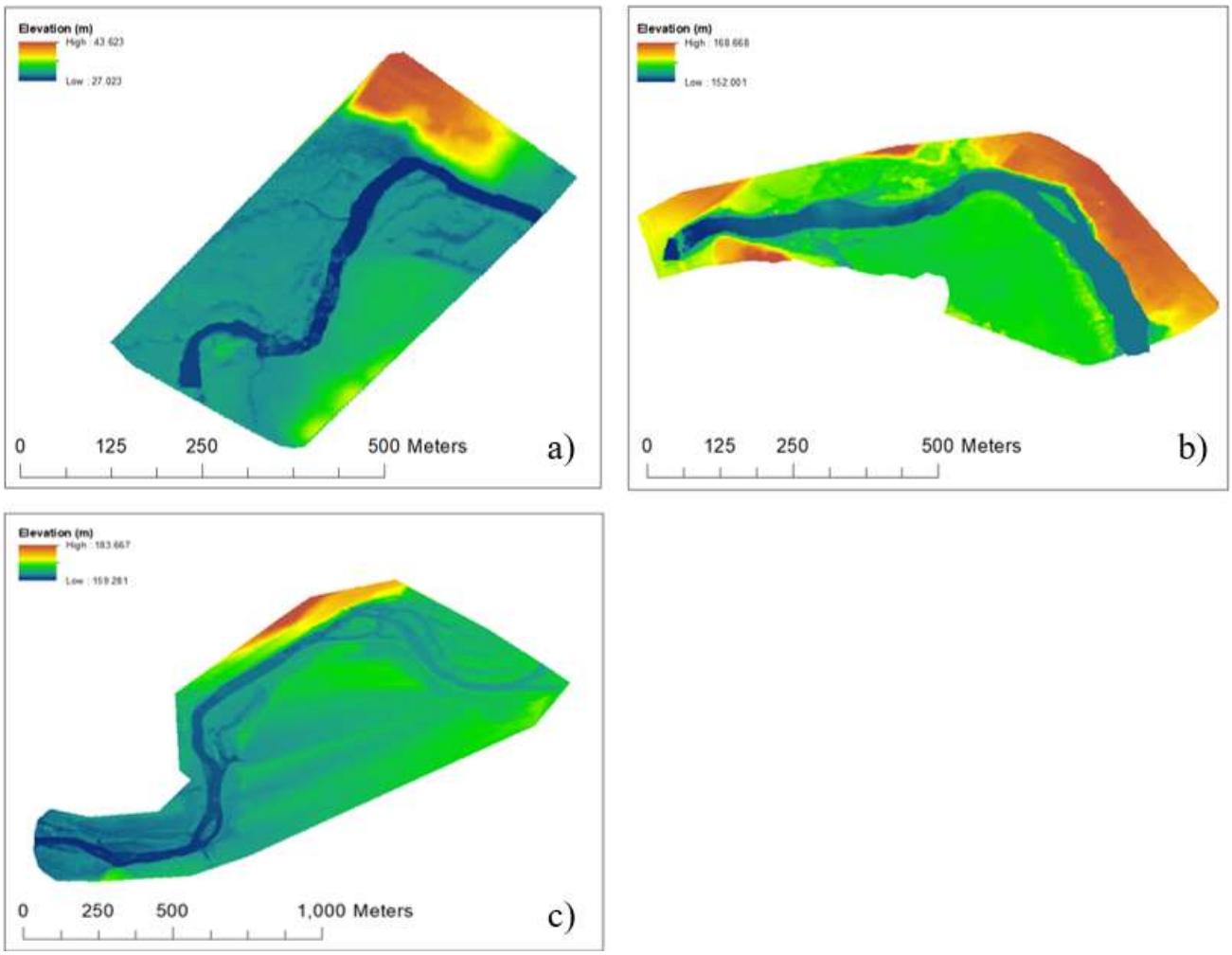

Figure 8. Merged DEMs for each focal study site created from LiDAR and surveying data: a) Lamprey River Site, b) Sugar Site 6, and c) Sugar Site 2.

3.4.5 Modeling in FaSTMECH

Flow and Sediment Transport with Morphological Evolution of Channels (FaSTMECH; Nelson, 2013) is a quasi-steady two-dimensional model developed by the United States Geological Survey (USGS) available for public use through International River Interface Cooperative (iRIC) software. FaSTMECH uses the continuity and Navier-Stokes equations for the conservation of fluid mass and momentum to solve for velocity and shear stress for each cell within an orthogonal curvilinear grid (Nelson, 2013). Riverbed topography, discharge, lateral edge viscosity (LEV), and downstream stage are required inputs in the model (Nelson, 2013).

Table 3. Discharge values for each site based on the discharge measured at the USGS gauge stations and percentage of total watershed area draining to an individual site. The low discharge value represents the discharge during the day the riverbed was surveyed, the medium discharge is the highest discharge recorded during the study period, and the high value is the maximum discharge recorded within the past 20 years.

	Upstream Watershed Area (km2)	Low Discharge (cms)	Medium Discharge (cms)	High Discharge (cms)
Sugar Gauge Station	713.98	5.15	110.32	272.72
Lamprey Gauge Station	553.48	4.14	35.84	251.16
Sugar Site 2	624.39	4.51	96.48	238.50
Sugar Site 6	652.52	4.71	100.82	249.24
Lamprey Site	283.50	2.12	18.36	128.65

Topographic data in the form of a point cloud was imported into FaSTMECH (Figure 8). A topographic surface was created within the program using the attribute mapping figure along a curvilinear grid following the thalweg of the channel. A grid of 0.5 by 0.5-meter cells was used for Sugar Site 6 and the Lamprey Site, while 1.0 by 1.0-meter cells were used for Sugar Site 2, which was larger. The width of each grid was selected as the maximum width possible to trace the shape of the river channel while remaining within the bounds of the DEMs. The width was set to 100 meters for the Sugar Site 6 and the Lamprey Site and 200 meters for the larger Sugar Site 2.

The model was run at steady state for three discharges for each modeled focal site: a low, medium, and high flow, which represent the discharge during the day the riverbed was surveyed, the maximum discharge recorded within the study period, and the maximum flow level over the past 20 years, respectively (Table 3). The largest discharge over the past 20 years was selected as the high discharge value as it is a realistic scenario that each site experienced relatively recently. Discharge within each reach was scaled by multiplying discharge measured at the gauge station by the proportion of the area of the watershed upstream of each study site (Galster, 2007).

Downstream stage at each discharge was calculated using the Manning equation for Study Site 2 and the Lamprey Site (Arcement and Schneider, 1989):

$$Q = VA = \left(\frac{1}{n}\right) R^{2/3} S^{1/2}$$

where Q (m^3/s) is discharge, V (m/s) is flow velocity, A (m^2) is the cross-sectional area of the channel, n is the Manning's roughness coefficient, R (m) is the hydraulic radius of the channel, and S (m/m) is channel slope (Arcement and Schneider, 1989). The Manning's roughness coefficient was set to a value of 0.3 based on channel characteristics (Arcement and Schneider, 1989). Boundary conditions are displayed in Table 4.

The downstream boundary of Sugar Site 6 is a trapezoidal weir. Calculations for stage were completed using the weir equation (Brater and King, 1982):

$$Q = CLH^{3/2}$$

where Q (m^3/s) is discharge, C ($m^{0.5}s^{-1}$) is the discharge coefficient, L (m) is the length of the weir, and H (m) is the height of the water surface over the weir (Brater and King, 1982). A discharge coefficient of 1.7 $m^{0.5}s^{-1}$ was chosen based on the length, width, and shape of the dam (Brater and King, 1982). This particular weir is about 0.6 m wide and 30 m long and has a 6 m long rectangular notch inset for low flows. At higher discharges water exceeds the low-flow 6 m long notch to span the entire 30 m of the weir, increasing its length. Boundary conditions are displayed in Table 5.

Table 4. Boundary conditions for Sugar Site 2 and the Lamprey Site at each modeled discharge.

Site	Discharge (m^3/s)	Manning's n	Hydraulic Radius (m)	Channel Slope	Downstream WSE (m)
Sugar Site 2	4.51	0.03	0.36	0.0024	159.926
	96.48	0.03	0.86	0.0024	161.511
	238.5	0.03	0.87	0.0024	162.4305
Lamprey Site	4.71	0.03	0.23	0.0016	28.242
	100.82	0.03	0.76	0.0016	28.925
	249.24	0.03	0.74	0.0016	30.969

Table 5. Boundary conditions for Sugar Site 6 at each modeled discharge.

Site	Discharge (m^3/s)	C ($m^{0.5}\ s^{-1}$)	L (m)	H (m)	Downstream WSE (m)
Sugar Site 6	2.12	1.7	6	0.597421	160.097421
	18.36	1.7	30	1.575135	161.5751346
	128.65	1.7	30	2.879818	162.879818

In FaSTMECH, constant discharge and downstream stage were set for each reach based on the calculations above. Upstream stage was selected to minimize the mean error on discharge. The model was run under steady 2-D conditions to produce the distribution of velocity and shear stress in the streamwise curvilinear grid. Ten values of streamwise shear stress near each of the knotweed and native vegetation patches were extracted from the model results. Streamwise shear stress was selected over stream-normal shear stress in this analysis, as the locations of vegetation patches were mainly within straight channels where streamwise shear stress would be the dominant cause of fluvial entrainment on the banks (Bywater-Reyes et al., 2018). The estimated shear stress for each of three flow conditions was compared using Student's t-test to assess if either patch experienced notably different hydraulic conditions which could account for variations in erosion magnitude between patches. The shear stress values were also compared to calculated critical shear stress values based on soil properties of the banks (Julien and Torres, 2006). To verify the accuracy of the model, the water surface elevation (WSE) calculated by the

model for the discharge in the reach during surveying was compared with surveyed WSE values using a Student's t-test.

Additional model runs were conducted in order to determine the discharge associated with stage levels which fully submerged each set of top, middle, and bottom bank at each focal site. This was done in order to assess how often parts of the bank were being effected by applied shear stress and would potentially erode due to fluvial entrainment.

3.5 Testing Soil Characteristics

Many factors contribute to the erodibility of a riverbank, including soil properties and the presence of vegetation (Julian and Torres, 2006; Mahalder et al., 2018). To characterize the extent to which soil properties were similar among vegetation patches at each site, soil properties, including soil moisture, bulk density, grain size distribution, and critical shear strength, were estimated for each vegetation patch at the three focal study sites. While many methods, including in-situ and laboratory testing, have been developed to quantify the critical shear stress, this study used an empirical equation that had been developed for rivers with similar characteristics (grain size distribution, and moisture content) to the study rivers (Hanson, 1990; Julien and Torres, 2006; Wahl, 2016; Mahalder et al., 2018).

To collect the soil samples, a 2-inch polyvinyl chloride (PVC) pipe was inserted laterally into the riverbank using a sledgehammer. The PVC pipe was then capped using a test plug to create suction during pipe removal. The amount of soil recovered within the pipe was measured. This was done using a measuring tape to record the distance from one end of the pipe to the beginning of soil at the inside top and the inside bottom of the pipe. The two values were then averaged and subtracted from the overall length of the pipe to obtain the average length of soil in

the pipe, which was used to calculate the volume of recovered soil using the equation for the volume of a circular cylinder. The soil removed from the bank was stored in airtight bags in a refrigerator until it was tested.

Every soil sample was weighed at the start of testing. The weight of the wet soil was divided by the volume of the soil collected in the pipe to calculate wet bulk density (Mahalder et al., 2018). Next, each soil sample was dried in an oven at 105 degrees Celsius for 24 hours (Matthes et al., 1992; Tanner and Leong, 1995). Once dry, samples were weighed again to obtain the dry weight of the samples (Matthes et al., 1992; Tanner and Leong, 1995). The difference in weight between the wet and dried sample was divided by the weight of the wet sample to calculate the moisture content of the soil (Matthes et al., 1992; Tanner and Leong, 1995). All weighing was performed on a Mettler Toledo PB303, which reports values to the nearest milligram.

Each dry soil sample was then wet sieved using a 63-µm sieve until the reverse osmosis water running through the sample was clear (Matthes et al., 1992; Tanner and Leong, 1995). This process removed silt and clay particles leaving only sand behind (Matthes et al., 1992; Tanner and Leong, 1995). The sediment remaining in the sieve was collected and dried in an oven at 105 degrees Celsius for 24 hours before being re-weighed and recorded as the weight of dry sand in each sample (Matthes et al., 1992; Tanner and Leong, 1995). The dry weight of silt and clay within the sample was calculated by subtracting the weight of dry sand from the total sample dry weight. This value was then divided by the total weight of dry sediment to obtain the silt-clay fraction of the soil.

Finally, critical shear stress was estimated using a rating curve that had been developed for soils in Aiken, South Carolina (Julian and Torres, 2006), which have similar percentages of

silt and clay, along with soil moisture, as the study soils (Web Soil Survey). Silt-clay percentage was used to calculate the critical shear stress of the soil in the following third-order polynomial equation where τ_c (Nm^{-2}) is the critical shear stress of the soil and SC% is the silt-clay percentage content of the soil (Julien and Torres, 2006):

$$\tau_c = 0.1 + 0.1779(SC\%) + 0.0028(SC\%)^2 - 2.34e^{-5}(SC\%)^3$$

Critical shear stress was then compared between vegetation patches using a Student's t-test. The critical shear strength of the bank was compared to the applied shear strength of the water on the bank predicted by the model, to see if the predicted applied shear stress would exceed the critical shear stress of the bank, making it susceptible to erosion (Julian and Torres, 2006).

Chapter 4: Results and Discussion

4.1 Knotweed Survey

Knotweed patches were found throughout sections of both rivers (Figure 9; Figure 10). Knotweed appeared to be more common near urban areas and less common in sections of the river further away from infrastructure (Figure 9; Figure 10), which is consistent with previous studies (Duquette et al., 2016). The Lamprey River was floated across two visits; a section of the Lamprey River from Epping, NH to Wadleigh Falls, Lee, NH was floated on April 18th, 2021, and a section spanning from Raymond, NH to Epping NH, was floated on May 5th, 2021. In total, 26 patches of knotweed were identified along 26 kilometers of the Lamprey River. Throughout the 21-kilometer section of the Sugar River floated on June 1st, 2021, 50 patches of knotweed were identified. Knotweed patches were usually dense, though a few sparse patches were observed, especially in locations that appeared to be newly established. The locations of the

knotweed patches were uploaded to EDDMapS, which is used by the state of New Hampshire to monitor the spread of invasive plant species.

The presence of knotweed on both rivers should be a concern to local watershed management (Colleran and Goodall, 2014; Colleran and Goodall, 2015; Colleran et al., 2020). Knotweed is highly invasive and has potential implications on fluvial ecosystems and geomorphology (Lavoie, 2017; Drazan et al., 2021). While knotweed is difficult to remove, removing it while knotweed populations along a river are relatively low can prevent the need for more extensive and expensive remediation efforts later on, such as installing riprap along banks and reconstructing piers that have been subject to erosion (Colleran et al., 2020).

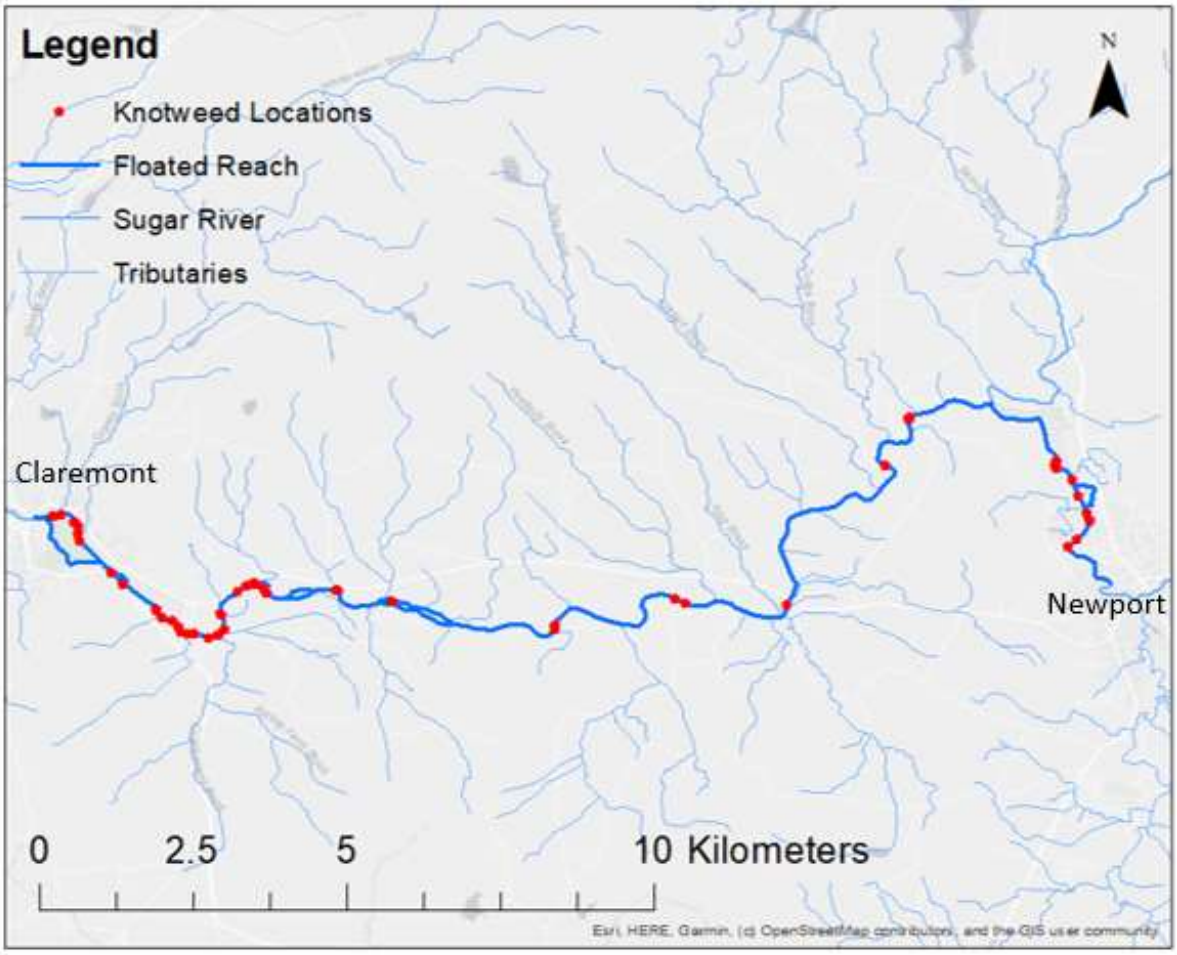

Figure 9. Identified locations of Itadori knotweed along the Sugar River, which flows from east to west. Knotweed was more commonly found near the urban areas of Claremont and Newport, NH. Reaches shown in dark blue were assessed during the current study; reaches in light blue were not assessed.

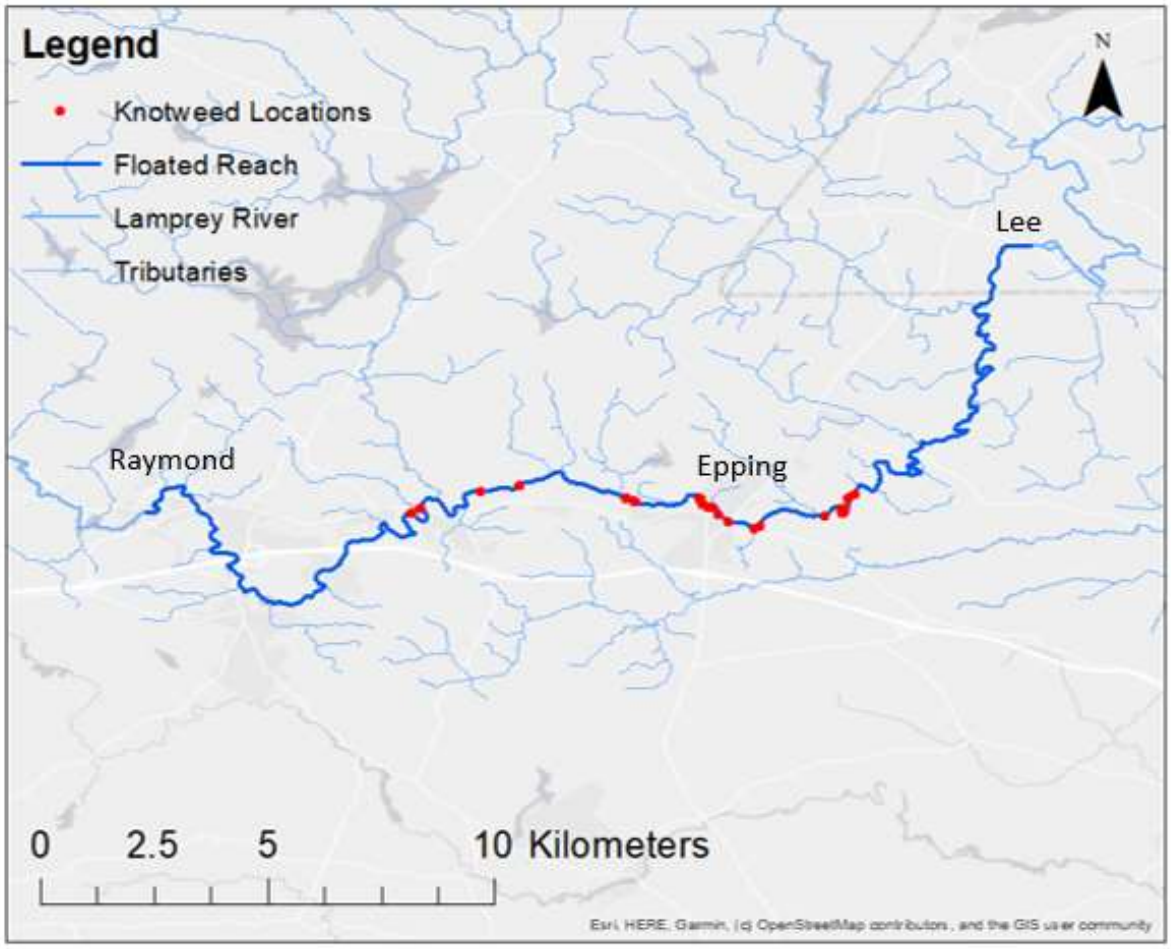

Figure 10. Identified locations of Itadori knotweed along the Lamprey River, which flows from west to east. Knotweed was most commonly found near the urban area of Epping, NH. Reaches shown in dark blue were assessed during the current study; reaches in light blue were not assessed.

4.2 Erosion Monitoring Results

4.2.1 Results of Erosion Monitoring Using Bank Pins

Over the entire study duration, bank areas covered with knotweed experienced more erosion than bank areas covered with native vegetation (Figure 11). More specifically, bank pins located in knotweed patches experienced more erosion than those located in native vegetation patches when using data from all sites ($p = 0.002$, $N = 122$) and when only using sites without recovered bank pins ($p < 0.001$, $N = 48$). Banks with knotweed were observed to erode more on average compared to those without, which supports the results of past studies (Mummigatti, 2008; Arnold and Toran, 2018; Hammer, 2019; Matte et al., 2021). Overall, when using data from all sites, bank pins installed in knotweed patches had an average of 11.1 cm (SD = 8.92 cm) of erosion, compared to pins in native vegetation patches, which had an average of 4.33 cm (SD = 8.12 cm). Knotweed patches had an average of 4.3 cm more erosion than native patches when looking at only sites without unrecovered bank pins. In addition, it was found that the position of a bank pin on the bank did not impact the amount of erosion it experienced. There was no statistically significant difference was found between erosion rates experienced by pins placed in upstream as opposed to downstream columns, or between top, middle, and bottom pins (Figure 11). Raw bank pin data is displayed within Table 10.

Some bank pins were not recovered in their original location. It is likely that unrecovered bank pins were potentially pulled out or bent by ice jams or large woody debris or removed by mass failure of the bank. Out of the focal study sites, Sugar Site 6 was the only one to have unrecovered bank pins. Two pins were lost between December 10th, 2021, and April 29th, 2022, when flows were the highest and there was the potential for ice jams. Ice jams or large woody

debris were suspected to have pulled out the missing pins because some of the recovered pins had been bent. Sugar Sites 3 and Sugar Site 5 both had missing pins during the final site visit on September 29th, 2022. In these cases, there was evidence of mass failure of bank material. The bank at Sugar Site 3 was originally very steep at around a 90-degree angle during the installation of the pins; the following year, the bank was sloped at around a 60-degree angle. At Sugar Site 5, a large chunk of the bank appeared to have collapsed from the top of the bank; one bank pin was found buried within the collapsed bank material. Even when these sites with unrecovered bank pins were completely removed from the analysis, knotweed patches were still found to experience more erosion than native patches in when only using sites without recovered bank pins ($p < 0.001$, $N = 48$).

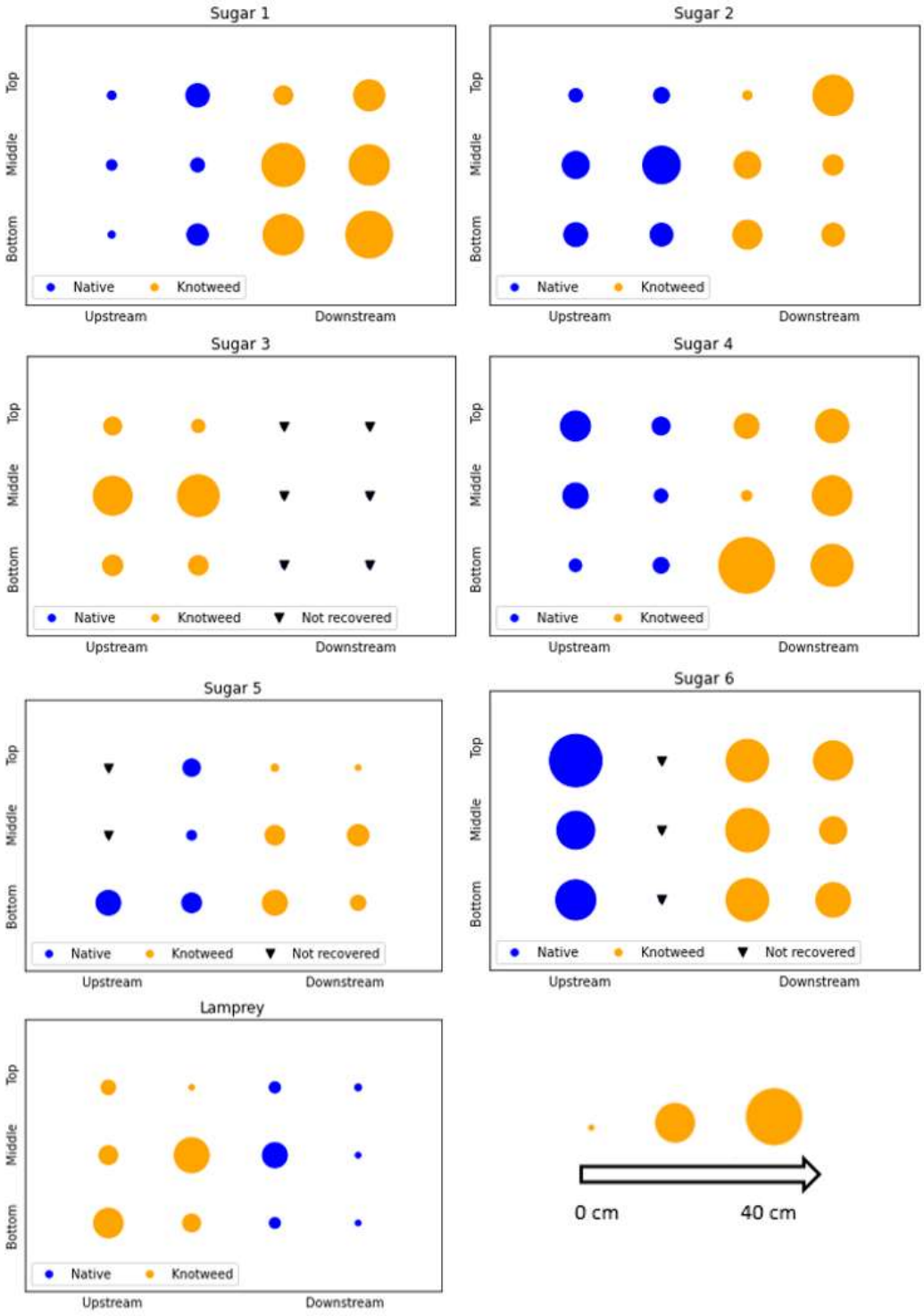

Figure 11. Total change in the amount of bank pin exposed between the first and last site visit for each bank pin. Pins that were missing from the bank during the last site visit are marked with a black triangle. Blue indicates native vegetation and orange indicates knotweed. The size of each circle corresponds to the amount of change that was observed.

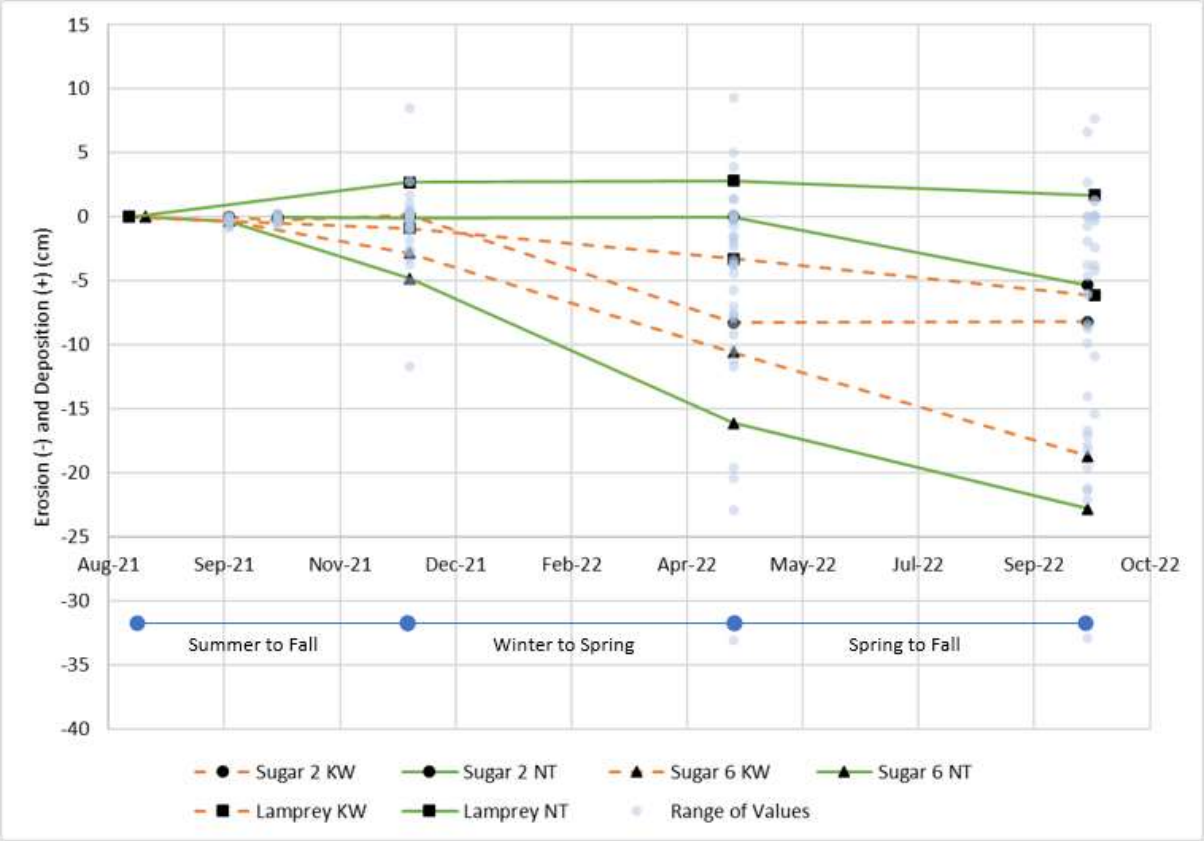

Figure 12. Cumulative bank erosion and deposition recorded at each site visit to the three focal sites showing how erosion rates changed throughout the study period. Grey dots show the cumulative erosion and deposition recorded at individual pins throughout the study period. Seasonal time periods correspond to Table 6.

Table 6. Seasonal erosion and deposition rates recorded at each focal study site. Erosion rates were calculated by dividing the average erosion rates at each vegetation patch throughout each time period by the number of months within each time period. Time periods were selected based on dates of site visits. Positive values indicate deposition.

Site	Summer 2021 to Fall 2021 (cm/month)	Winter 2021 to Spring 2022 (cm/month)	Spring 2022 to Fall 2022 (cm/month)
Sugar 2 Native	-0.01	-1.14	0.26
Sugar 2 Knotweed	0.06	-1.80	0.01
Sugar 6 Native	-0.87	-2.42	-1.31
Sugar 6 Knotweed	-0.52	-1.66	-1.59
Lamprey Native	0.67	0.03	-0.22
Lamprey Knotweed	-0.22	-0.51	-0.55

A seasonal variation in erosion rates was observed for focal sites ($p = 0.001$), which were visited multiple times throughout the study period (Figure 12). There was no difference found in seasonal erosion rates between knotweed and native vegetation patches ($p = 0.269$). Within the study period of August 2021 to October 2022, the most erosion took place between Winter 2021 and Spring 2022 for all vegetation patches except the native and knotweed patch at the Lamprey Site (Figure 12; Table 6).

The increase in erosion noted during site visits in December 2021 and April 2022 compared to earlier site visits correspond to overall high discharge levels during winter and early spring months of 2022, as shown in the hydrographs for the Lamprey and Sugar Rivers (Figure 7; Figure 12). Higher amounts of erosion observed during winter and early spring months (Figure 12; Table 6) is consistent with other studies that also noticed increasing erosion during the winter months (Arnold and Toran, 2018, Matte et al., 2021). During the winter months, riverbanks in the northeastern United States not only are subjected to higher river discharge, but also experience freeze-thaw cycles, which can weaken the bank material (Chassiot et al., 2020). In addition, both study rivers showed evidence of ice jams or large woody debris impacting the bank pins; ice jams can abrade bank material causing erosion (Chassiot et al., 2020).

Additionally, the number of days each bank pin at the focal sites was submerged was estimated in order to analyze how much the bank material near each pin elevation, top, middle, or bottom, was subjected to potential fluvial entrainment. This was done using stage estimates developed using the hydraulic model at various discharges compared to the elevation of each bank pin. The bottom pins were submerged approximately 315 days, 295 days, and 215 days, the middle pins were submerged approximately 75 days, 58 days, and 45 days, and the top pins were submerged approximately 9 days, 16 days, and 9 days, respectively for Sugar Site 2, Sugar Site

6, and the Lamprey Site. Top, middle, and bottom bank pins experienced similar amounts of erosion overall but were not equally subjected to the applied shear stress which causes fluvial entrainment. The lack of difference in observed erosion at different bank elevations suggests that fluvial entrainment is not the dominant erosional mechanism on the banks of the focal sites.

4.2.2 Monitoring Bank Erosion Using Structure from Motion

Using the Structure from Motion (SfM) technique proved challenging in study sites. During the summer and falls visits, the sites had dense vegetation cover making it difficult for photographs to capture the bank surface and for the photos to be processed by Pix4D (Table 1). No successful leaf-on point clouds were created for any of the patches at the three focal sites. The dense vegetation made it impossible for geospatial software to patch together a continuous surface of the bank profile. During the December 10th, 2021 and April 29th, 2022 visits, the SfM technique was limited by river access (Table 1). High river stage but incomplete ice cover prevented mid-channel access, limiting the number of angles and distance from the bank from which photographs could be acquired. High flows at the time of drone flights limited the amount of bank able to be reconstructed using SfM and compared to other datasets. During one of the visits, on December 10th 2021, snow covered the banks, eliminating the potential to use SfM to accurately record bank surface topography (Table 1). Future bank erosion studies using SfM should consider vegetation cover of the bank as well as seasonal changes in river flow patterns and local weather when planning site visits.

In the future, if photographs are obtained during summer months, then it is recommended that this technique be used exclusively on banks with limited vegetation cover, or during winter months when vegetation cover is limited on banks. When site access by foot is limited, other

techniques, such as using drones or attaching a camera to a pole, may allow for better coverage of the banks (Jugie et al., 2018; Chassiot et al., 2020).

4.3 Site-specific Vegetation Survey Results

Vegetation at all study sites primarily consisted of dense herbaceous vegetation or shrub-saplings. Native vegetation patches of the Sugar River focal sites were dominated by *Solidago flexicaulis* and *Boehmeria cylindrica* (Table 7). The native patch at the Lamprey Site was dominated by *Cornus amomum* (Table 7). While most native vegetation patches had multiple species present in each patch, knotweed patches were typically monocultures, except for knotweed plot 1 at Sugar Site 2 which included one stem of *Solidago flexicaulis* (Table 7). Native vegetation at the non-focal sites was mainly dense shrubs and saplings, except for Sugar Site 3 which was mainly grass. Knotweed patches were dense monocultures at all non-focal sites. Native patches of Sugar Site 2, Sugar Site 6, and the Lamprey Site had Shannon diversity index scores of 0.846, 0.824, and 0.108, respectively. Knotweed patches of Sugar Site 2, Sugar Site 6, and the Lamprey Site had Shannon diversity index knotweed patches of 0.127, 0.0, and 0.0, respectively. The was no difference in species diversity ($p = 0.089$) using the Shannon diversity index between knotweed and native vegetation patches. There was a notable change in vegetation cover between summer and winter seasons (Figure 13). Both herbaceous and shrub-sapling vegetation and knotweed likely died back at all study sites over the winter months.

Table 7. Vegetation survey results for the three focal study sites. Three one-meter square quadrats were surveyed at each vegetation patch. Plot 1 represents the most upstream quadrat in a patch, plot 2 was centered over the bank pins, and plot 3 was the most downstream quadrat.

	Sugar Site 2		**Sugar Site 6**		**Lamprey Site**	
Quadrats	**Species**	**Stem Count**	**Species**	**Stem Count**	**Species**	**Stem Count**
Native 1	*Boehmeria cylindrica*	1	*Athyrium filix-femina*	4	*Cornus amomum*	73
	Celastrus scandens	1	*Boehmeria cylindrica*	18	*Solidago flexicaulis*	2
	Solidago flexicaulis	45	*Solidago flexicaulis*	23		
Native 2	*Athyrium filix-femina*	7	*Boehmeria cylindrica*	10	*Cornus amomum*	57
	Boehmeria cylindrica	1	*Fraxinus nigra*	1	*Solidago flexicaulis*	1
	Robinia pseudoacacia	1				
	Solidago flexicaulis	9				
Native 3	*Ambrosia artemisiifolia*	1	*Boehmeria cylindrica*	35	*Boehmeria cylindrica*	1
	Boehmeria cylindrica	14	*Solidago flexicaulis*	7	*Cornus amomum*	69
	Solidago flexicaulis	10			*Solidago flexicaulis*	4
Knotweed 1	*Reynoutria japonica*	13	*Reynoutria japonica*	13	*Reynoutria japonica*	18
	Solidago flexicaulis	1				
Knotweed 2	*Reynoutria japonica*	11	*Reynoutria japonica*	15	*Reynoutria japonica*	7
Knotweed 3	*Reynoutria japonica*	12	*Reynoutria japonica*	8	*Reynoutria japonica*	10

Figure 13. a) Sugar Site 2 knotweed patch on September 29th, 2022, b) Sugar Site 2 knotweed patch on September 29th, 2022, c) Sugar Site 2 native patch on April 29th, 2022, and d) Sugar Site 2 native patch on April 29th, 2022.

4.4 Hydraulic Modeling of Erosion Susceptibility Results

The 2-D hydraulic model FaSTMECH appeared to provide reasonable estimates of flow within the focal study site reaches. More specifically, the modeled water surface elevation values were close to field measurements. For the Sugar Site 2, Sugar Site 6, and the Lamprey Site there was an average difference of 0.05 m, 0.08 m, and 0.123 m with a standard deviation of 0.257 m, 0.096 m, and 0.376 between ten model output WSE values and field WSE measurements at the same discharge, respectively. Due to site access and study duration limitations, field measurements of water surface elevation were only obtained during low flow periods; validation was thus not performed at higher discharges.

Applied shear stress computed by the model varied greatly between sites and discharges (Figure 20). Streamwise shear stress increased between the low, medium, and high discharges for all study sites (Table 8), even though the flow became overbank flow for the highest discharges (Figures 13-19). Sugar Site 2 experienced the highest applied streamwise shear stress around the vegetation patches (Figure 14; Figure 17). Sugar Site 6 had the lowest applied streamwise shear stress values (Figure 15; Figure 18). The Lamprey Site applied streamwise shear stress magnitudes were in between the values of the two Sugar River sites (Figure 16; Figure 19).

Applied shear stress was similar between paired knotweed and native vegetation patches at the same discharge (Table 8). More specifically, there was no statistically significant difference between the modeled shear stress results for knotweed patches when compared to native patches for any of the study sites ($p > 0.05$).

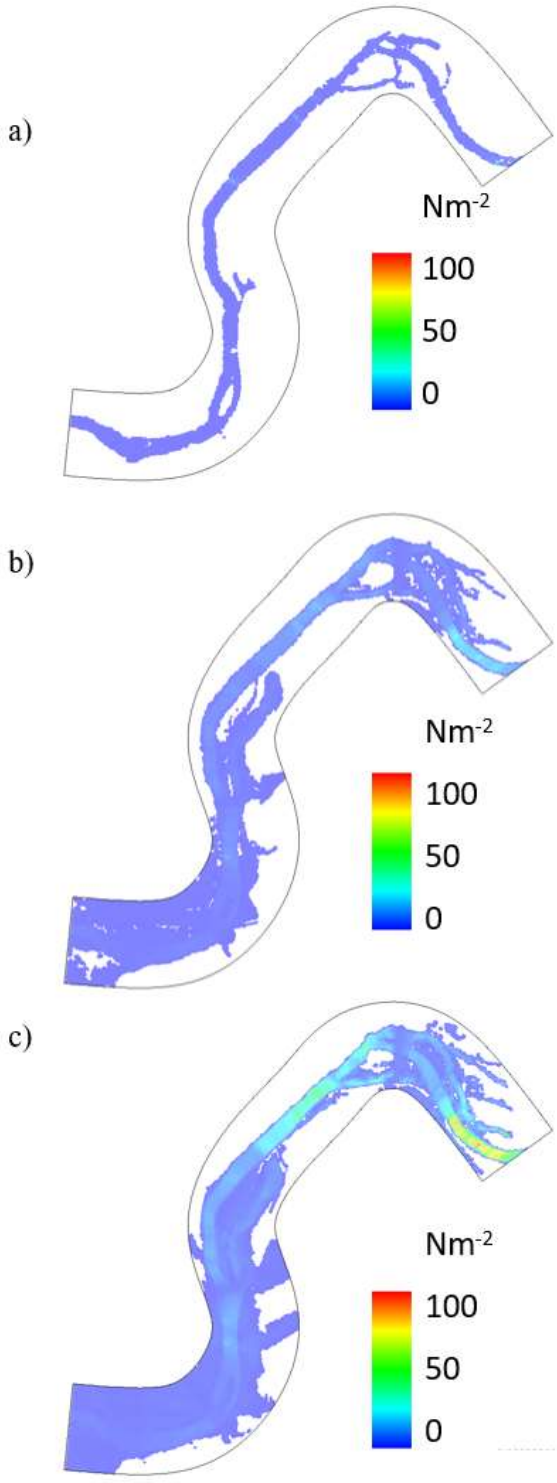

Figure 14. Model outputs showing shear stress (Nm^{-2}) in the streamwise direction for Sugar Site 2 at three different discharges, a) discharge on day of surveying, b) maximum discharge during the study period, and c) maximum discharge within the last 20 years. Direction of flow is from right to left. Note differences in color scale among subpanels.

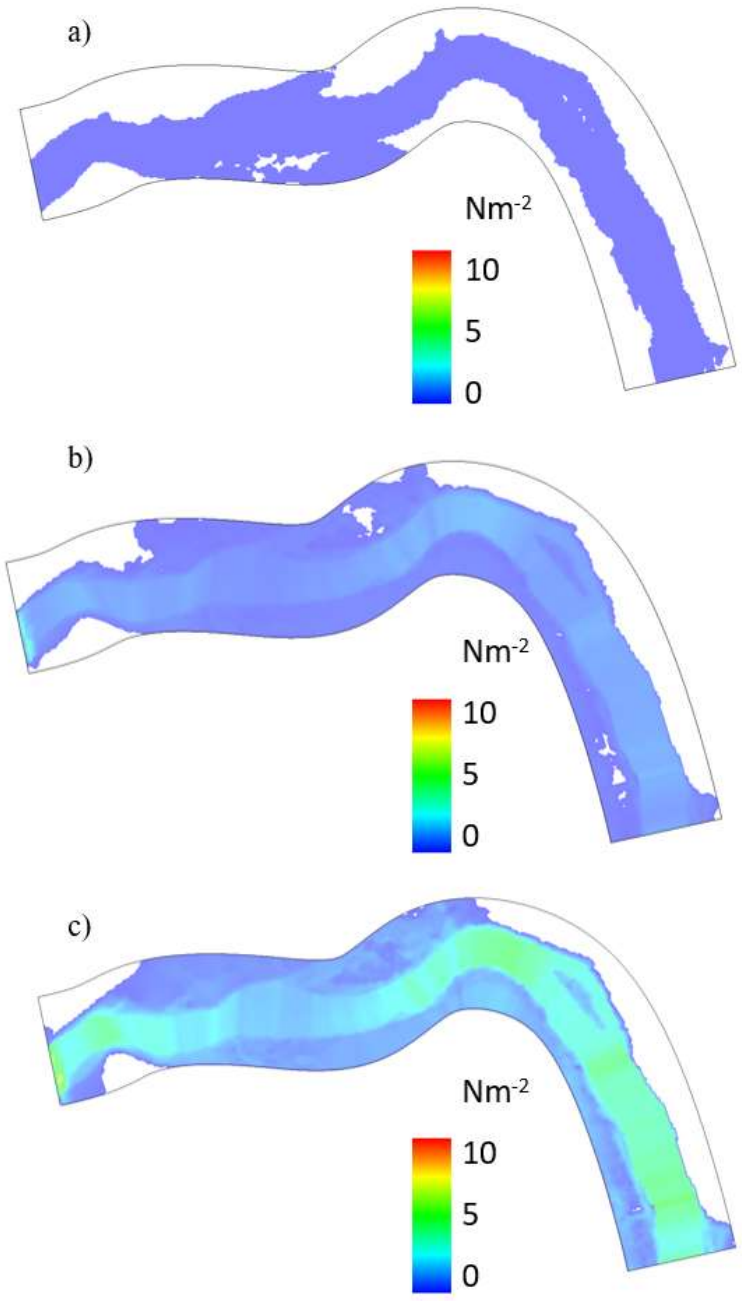

Figure 15. Model outputs showing shear stress (Nm^{-2}) in the streamwise direction for Sugar Site 6 at three different discharges, a) discharge on day of surveying, b) maximum discharge during the study period, and c) maximum discharge within the last 20 years. Direction of flow is from right to left. Note differences in color scale among subpanels.

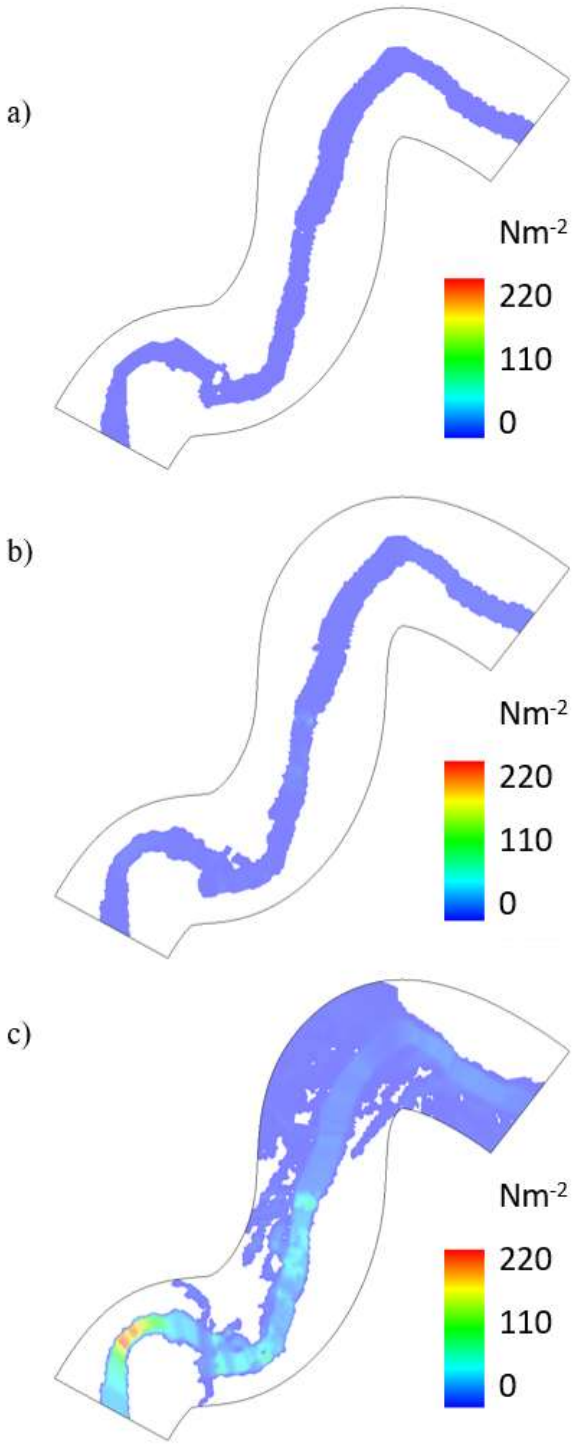

Figure 16. Model outputs showing shear stress (Nm^{-2}) in the streamwise direction for the Lamprey Site at three different discharges, a) discharge on day of surveying, b) maximum discharge during the study period, and c) maximum discharge within the last 20 years. Direction of flow is from left to right. Note differences in color scale among subpanels.

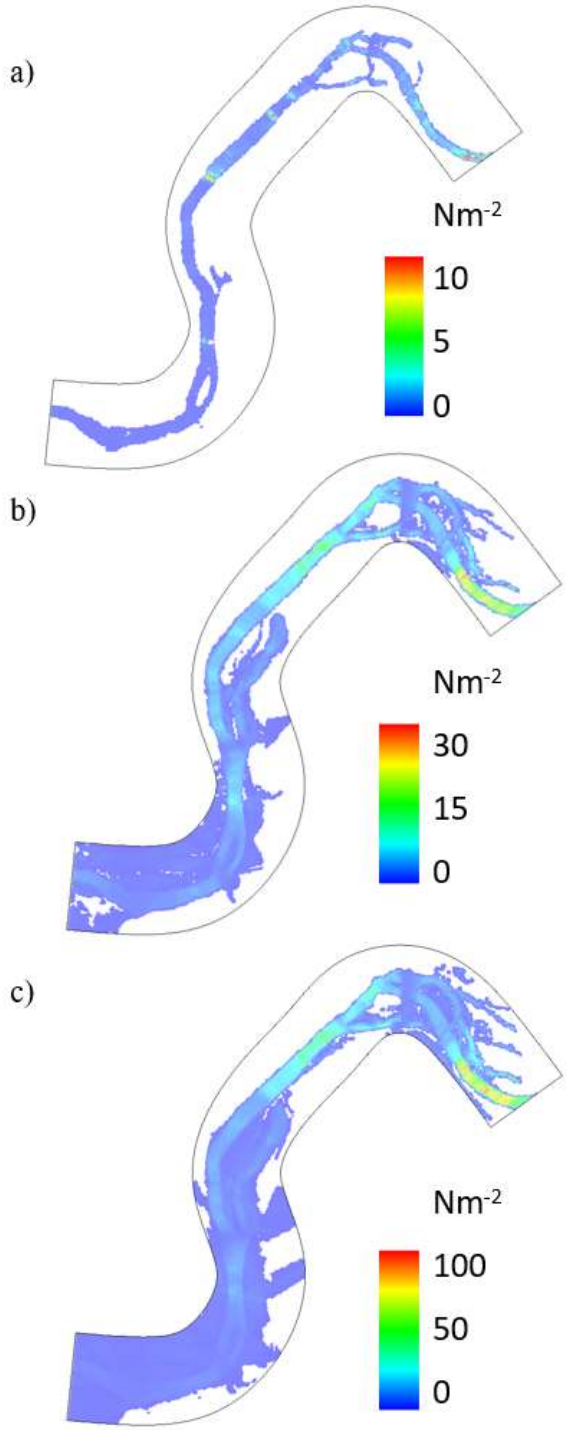

Figure 17. Model outputs showing shear stress (Nm^{-2}) at different scales in the streamwise direction for Sugar Site 2 at three different discharges, a) discharge on day of surveying, b) maximum discharge during the study period, and c) maximum discharge within the last 20 years. Direction of flow is from right to left. Note differences in color scale among subpanels.

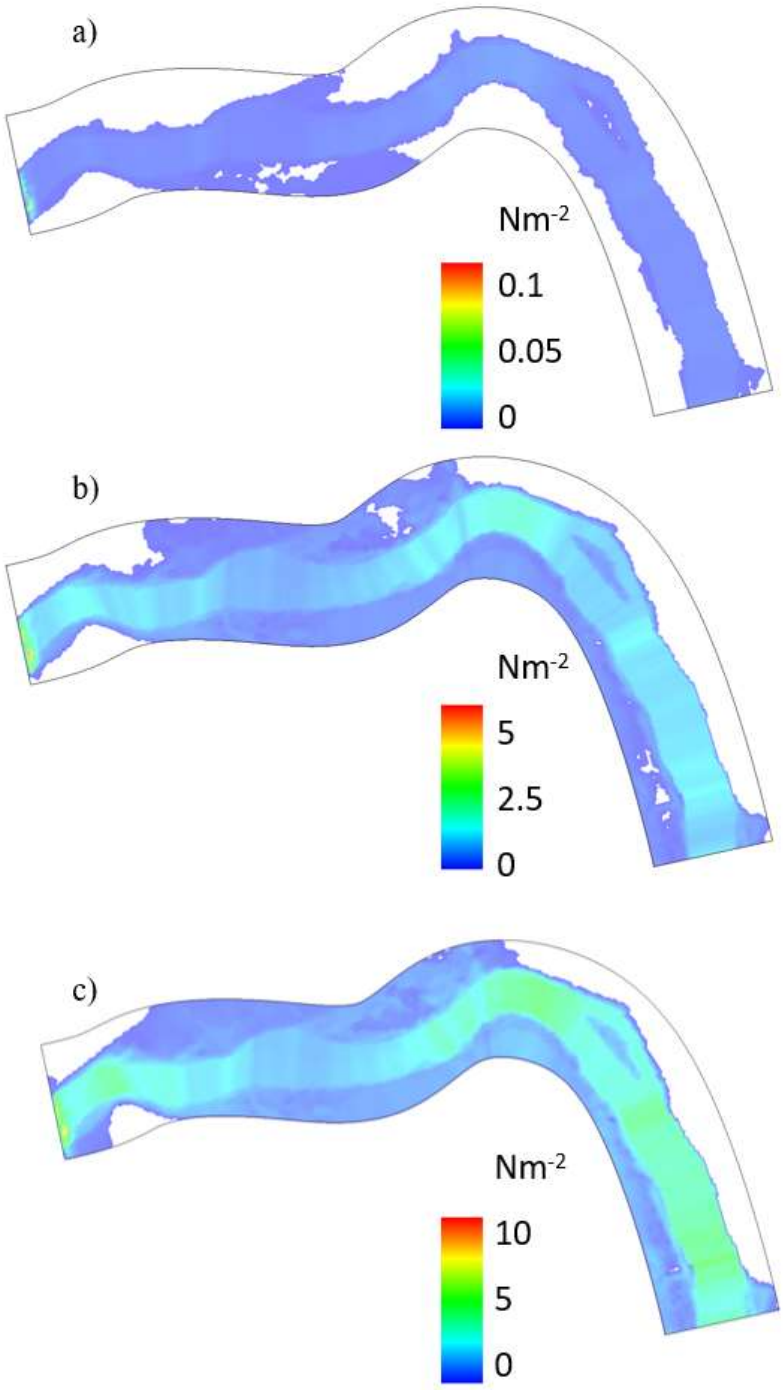

Figure 18. Model outputs showing shear stress (Nm^{-2}) at different scales in the streamwise direction for Sugar Site 6 at three different discharges, a) discharge on day of surveying, b) maximum discharge during the study period, and c) maximum discharge within the last 20 years. Direction of flow is from right to left. Note differences in color scale among subpanels.

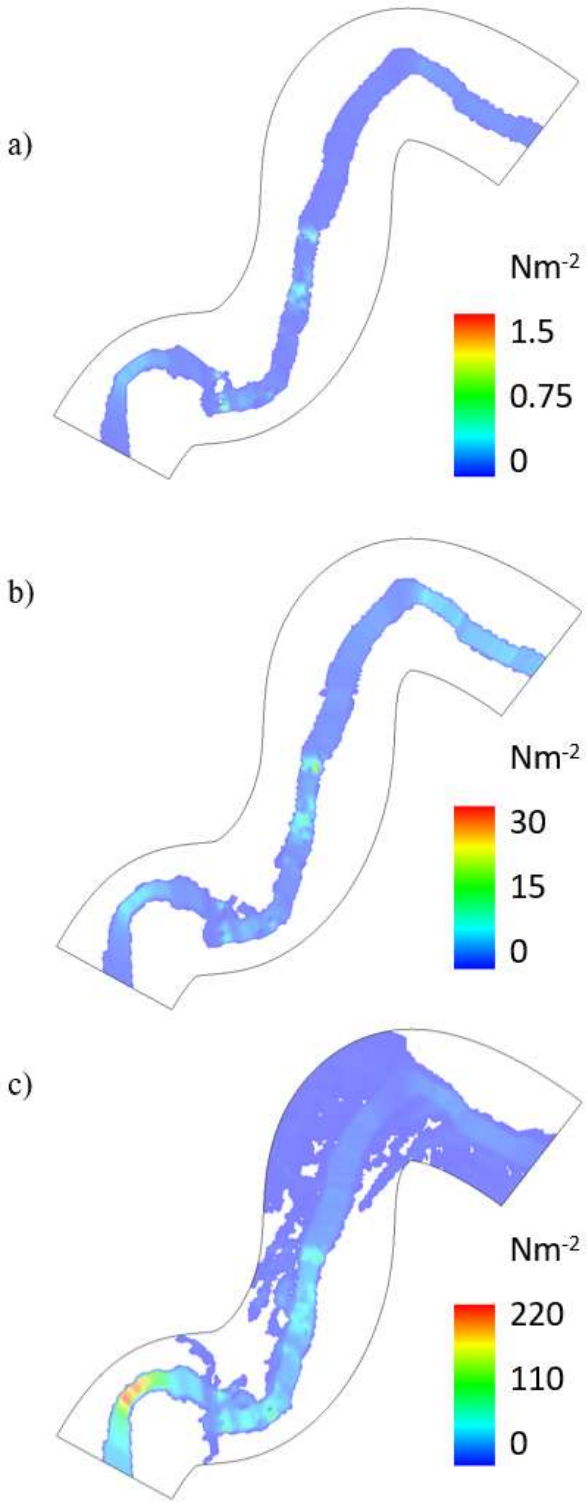

Figure 19. Model outputs showing shear stress (Nm^{-2}) at different scales in the streamwise direction for the Lamprey Site at three different discharges, a) discharge on day of surveying, b) maximum discharge during the study period, and c) maximum discharge within the last 20 years. Direction of flow is from left to right. Note differences in color scale among subpanels.

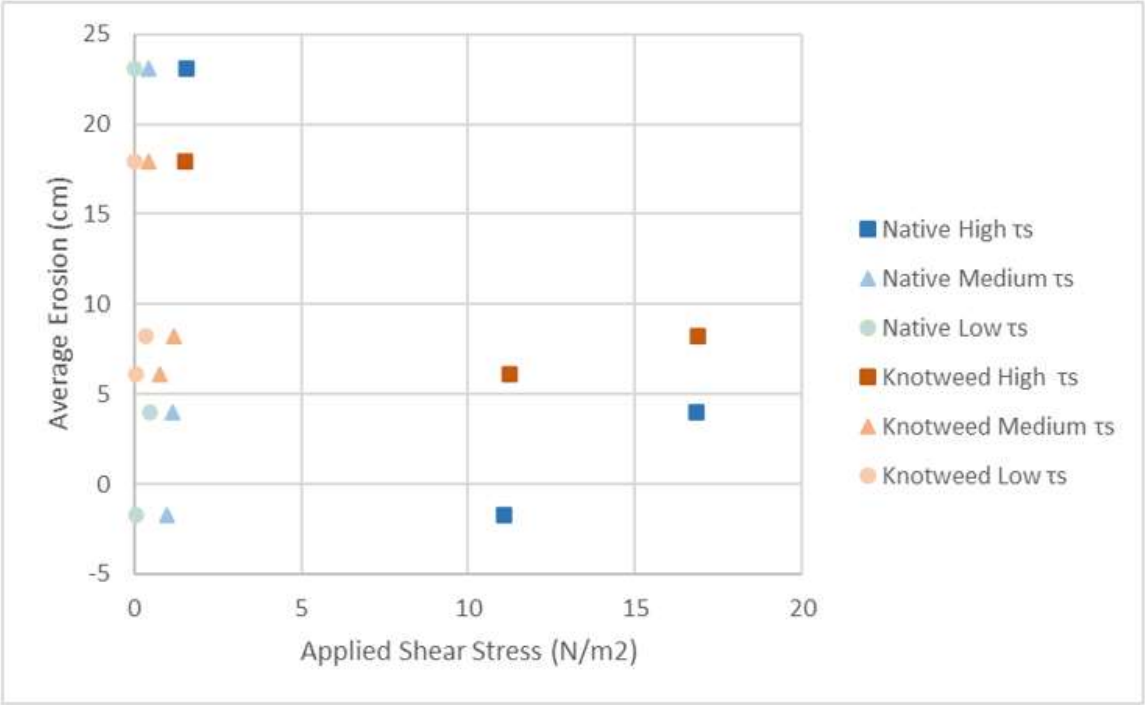

Figure 20. Average erosion compared to the applied shear stress at each focal site modeled at low, medium, and high discharges.

Table 8. Average applied streamwise shear stress (τ_s) and standard deviation (SD) calculated using streamwise shear stress values extracted from the FaSTMECH model outputs at each vegetation patch of the three focal sites. Low shear stress refers to the model output at the low discharge, the medium shear stress at the medium discharge, and high shear stress at the high discharge, as shown in Table 3. Values are the average across the ten model cells that were closest to each patch.

Sites	**Low τ_s (N/m^2)**		**Medium τ_s (N/m^2)**		**High τ_s (N/m^2)**	
	Average	**SD**	**Average**	**SD**	**Average**	**SD**
Sugar 2 Native	0.463	0.156	1.163	0.097	16.822	3.264
Sugar 2 Knotweed	0.363	0.295	1.180	0.230	16.878	4.887
Sugar 6 Native	0.003	0.001	0.412	0.168	1.544	0.180
Sugar 6 Knotweed	0.003	0.001	0.435	0.113	1.507	0.248
Lamprey Native	0.041	0.011	0.962	0.416	11.083	5.221
Lamprey Knotweed	0.059	0.027	0.778	0.552	11.250	3.698

4.5 Soil Characteristics

Soil characteristics were mostly similar across each pairing of vegetation patches. Silt-clay content, bulk density, soil moisture, and estimated critical shear stress, were mostly similar between knotweed and native vegetation patches at Sugar Site 2 (Table 9). The Lamprey Site had differences in bulk density and soil moisture content between vegetation patches (Table 9). The knotweed patch of Sugar Site 6 had a higher silt clay content (59%) compared to the native patch with soil containing 32% silt-clay (Table 9). There were no significant differences in silt-clay percentage, bulk density, or soil moisture content between the soil of knotweed patches compared to native patches, but the silt-clay percentage of the knotweed patch of Sugar Site 6 and the soil moisture content of the native vegetation of the Lamprey Site were outliers when compared to all collected data.

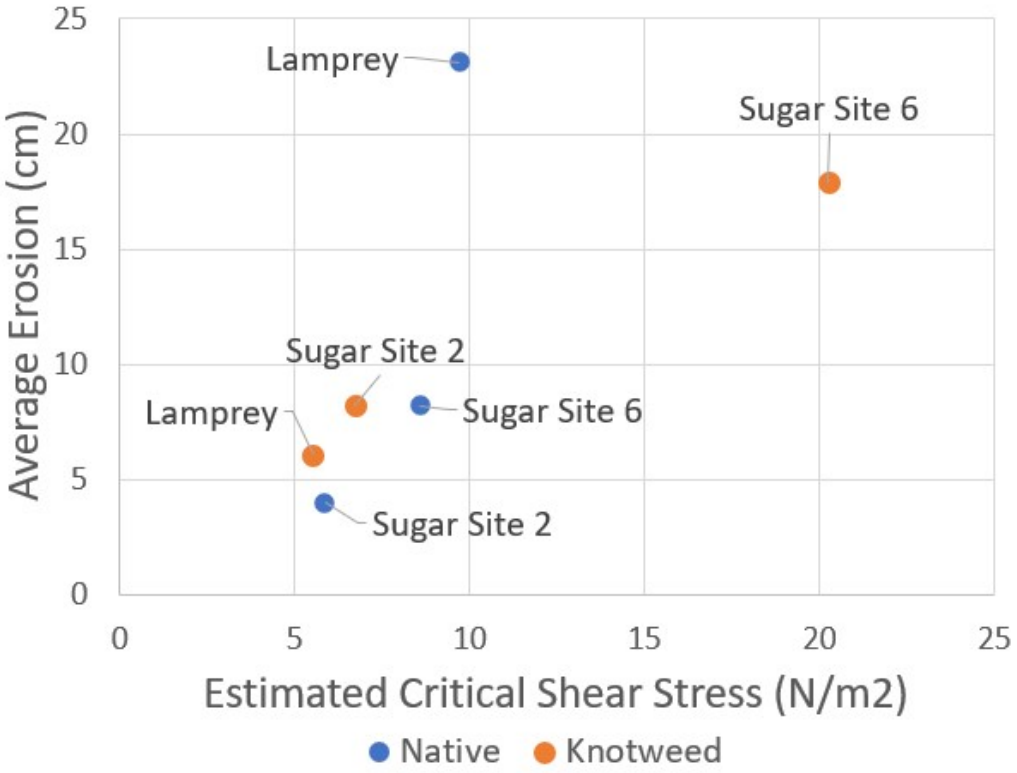

Figure 21. Average erosion compared to estimated critical shear stress values at each vegetation patch of the focal sites.

Table 9. Soil characteristics for each focal site vegetation patch. Shear stress was estimated using silt-clay % based on Julian and Torres (2006). Average erosion was calculated by averaging the total amount of erosion recorded over the entire study period at all bank pins within a vegetation patch.

Site Name	Silt and Clay %	Bulk Density (g/cm^3)	Soil Moisture Content (%)	Estimated Critical Shear Stress (N/m^2)	Average Erosion (cm)
Sugar Site 2 Native	24%	0.35	24%	5.85	4
Sugar Site 2 Knotweed	26%	0.35	24%	6.71	8.2
Sugar Site 6 Native	32%	0.39	24%	8.57	23.1*
Sugar Site 6 Knotweed	59%	0.32	19%	20.25	17.9
Lamprey Native	35%	0.28	57%	9.69	-1.7**
Lamprey Knotweed	22%	0.49	27%	5.52	6.1

* Not all bank pins we recovered.
** Negative values represent deposition.

Estimated critical shear stress ranged from 5.52 N/m^2 to 20.25 N/m^2 (Table 9). These values are higher than what was calculated using the same technique in Julien and Torres (2006) likely reflecting the higher percentage of silt and clay in the riverbank soils of the Lamprey and Sugar River. In addition, reported critical shear stress values only consider soil properties, not the effect of vegetation. Vegetation is suspected to increase critical shear stress in channel banks (Thorne, 1990).

In summary, the Lamprey site native patch had a slightly higher estimated critical shear stress than the knotweed patch. At both Sugar River sites, the native patch had a lower estimated critical shear stress. There was not a significant difference between estimated critical shear stress values at knotweed patches compared to native patches, but the estimated critical shear stress value at the Sugar Site 6 knotweed patch was an outlier (Figure 21). Overall, critical shear stress did not appear to be influencing erosion rates within the focal sites.

4.6 Comparison of Erosion Monitoring, Hydraulic Model Results, and Soil Characteristics

Overall, the only significant difference recorded between paired vegetation patches was the larger amount of erosion recorded at knotweed patches compared to native vegetation patches. No statistically significant difference was recorded between modeled applied shear stress values between paired vegetation patches, meaning that any difference in erosion rates between paired vegetation patches should not be attributed to flow patterns around the vegetation patches. In addition, there was no statistically significant difference between estimated critical shear stress between paired vegetation patches, apart from Sugar Site 6. At Sugar Site 6, the knotweed patch had a significantly higher estimated critical shear stress, which could explain why at this site the knotweed patch experienced less erosion than the native patch (Table 9). Overall, the difference in measured erosion between paired patches, apart from potentially Sugar

Site 6, cannot be attributed to differences in the estimated critical shear stress of the soil. In summary, the results of the bank erosion monitoring, vegetation survey, estimated critical shear stress, and modeled applied shear stress results show that the only significant difference across all paired patches was the presence of Itadori knotweed and the increase in erosion measured at knotweed patches.

For most of the studied scenarios at the focal sites, the applied shear stress (from the numerical model) was lower than the critical shear stress (estimated from soil characteristics). The only two scenarios in which applied shear stress exceeded the critical shear stress were the Sugar Site 2 and the Lamprey Site high discharge scenarios (Figure 22), but these high discharges were not observed during the study period. Therefore, no erosion via fluvial entrainment was expected within the study period. However, erosion was observed during at least one period of time at all focal study sites (Figure 12). In addition, Sugar Site 6 had the most recorded erosion, but the lowest applied shear stress and the Lamprey Site experienced the least erosion but had the second highest applied shear stress values (Table 9; Figure 11). In short, higher calculated applied streamwise shear stress did not correspond to higher amounts of erosion (Figure 20). Additionally, there was no difference between the amount of erosion recorded by top, middle, and bottom bank pins although the top, middle, and bottom pins all experienced different amounts of exposure to fluvial entrainment. These findings suggest that fluvial entrainment was not the principal mechanism of bank erosion at these sites and that other processes, such as mass failure, were dominant.

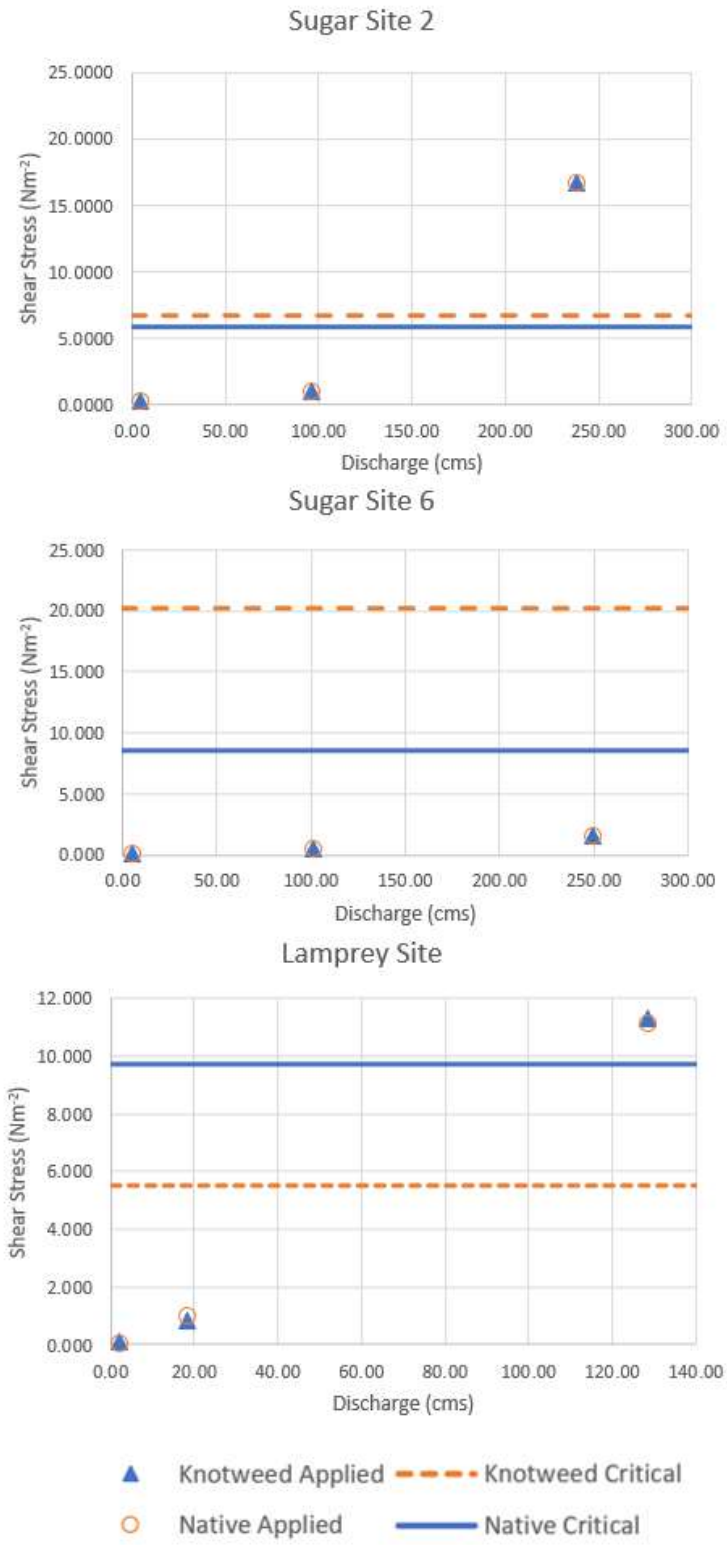

Figure 22. Calculated applied shear stress for knotweed and native vegetation patches at each of the three focal study sites. Critical shear stress values calculated based on bank soil properties are shown as horizontal lines in each plot.

Chapter 5: Conclusion

5.1 Summary of Findings

This study investigated the controls of bank erosion, including the impact of vegetation, on two New Hampshire rivers, concluding that the presence Itadori knotweed increases erosion rates on banks compared to native vegetation and that fluvial entrainment is not a dominant mechanism of erosion around knotweed patches. Multiple methods of studying bank erosion, including bank pins, SfM, and hydraulic modeling, were applied with varying levels of success. In general, vegetation patches were successfully paired based on estimated critical shear stress and modeled applied shear stress, only Sugar Site 6 had a significant difference between critical shear stress between vegetation patches. In situ bank pin observations provided further evidence that Itadori knotweed increases erosion rates compared to similar banks populated by native vegetation (Mummigatti, 2008; Arnold and Toran, 2018; Hammer, 2019; Matte et al., 2021). Increased erosion rates during winter and early spring months can be attributed to differences in temperature and flow patterns between seasons. This study further supports past work suggesting Itadori knotweed causes riverbank erosion and rules out the role of fluvial entrainment as a dominant mechanism of erosion near knotweed patches (Mummigatti, 2008; Arnold and Toran, 2018; Hammer, 2019; Matte et al., 2021).

5.2 Limitations

Limitations of this study include the small number of field sites. Field work, such as installing and monitoring bank pins and ground surveying, is time-consuming, and work with UAVs is costly, which limited the number of study sites in this study. This study was only conducted on two similar rivers, in terms of watershed area, slope, and substrate material, that

are located relatively near each other within similar climates. Extrapolating results to rivers with different geologic provinces or within different climates should be done cautiously, as rivers with larger watershed areas may experience more erosion due to high discharges, more riverbank erosion is expected in steeper rivers as flow velocity is usually higher, and bank and bed material can vary between rivers and impact erosion patterns.

There are many controls of bank erosion and, especially within field studies, it is challenging to isolate one dominant cause of bank erosion in specific locations (Lawler, 1995; Chassiot et al., 2020). While attempts were made to minimize differences in characteristics affecting bank erosion, such as bank height, soil type, local flow patterns, and vegetation density, between paired knotweed and native vegetation patches, it cannot be concluded that the only difference in erosion between paired vegetation patches was the presence of knotweed.

This study was limited to one year of data collection in the field. One year of data collection may not be representative of the river over a longer time. Moreover, New Hampshire experienced mild drought conditions throughout the summer and fall of 2022, which reduced the flow levels of the rivers and likely reduced erosion rates at the study sites. Short study periods are also unlikely to experience large rare floods, such as the 10-year or 100-year flow rate, which can cause a great amount of bank erosion and geomorphic change within a short period of time. In the future, longer-term and larger-scale research would be beneficial to better assess the impact of knotweed on erosion. There is potential for future work to combine remote sensing techniques such as UAVs or satellite imagery to increase the area and length of time being studied. For example, aerial imagery could be used to locate knotweed patches along entire river corridors, and repeat LiDAR elevation data could be used to estimate erosion and deposition at reach scales (Martin et al., 2018; Hamshaw et al., 2019).

Another study limitation is that bank pins may not be best suited to studying bank erosion in climates with cold winters where rivers may freeze, because ice jams as well as freeze-thaw processes in the bank may cause the movement of bank pins (Lawler, 1993; Couper et al., 2002). They also may interfere with natural bank processes by stabilizing or destabilizing the bank material or interfering with nearby hydrologic conditions. Visiting the sites to monitor erosion can also unnaturally impact the bank (Thorne, 1982; Lawler, 1993; Couper et al., 2002). Past studies have described "pin craters" where material directly surrounding the pin is disturbed leaving small indentations in the bank around the pin (Thorne, 1982); these were observed surrounding several bank pins within this study.

Another limitation of bank pins is their inability to capture bank change at locations in between where pins are installed (Jugie et al., 2018). Mass failure, like that observed within Sugar River Sites 3 and 5, is also difficult to monitor using bank pins, which are best suited to measuring fluvial erosion, which is the abrasion of the bank material by flowing water (Couper et al., 2002). While there are limitations in the use of bank pins to study erosion, it is still one of the most widely used methods to study riverbank erosion, due to its low cost and applicability to a wide range of fluvial environments and studies (Lawler, 1993; Couper et al., 2002; Foucher et al., 2016; Arnold and Toran, 2018). Another option is using Photo-Electronic Erosion Pins (PEEPs), which continuously track riverbank retreat using exposure to light (Lawler and Leeks, 1992). These can be useful to study erosion during particular time periods and around large flood events without the need to visit the sites in dangerous conditions (Lawler and Leeks, 1992). Instead of bank pins, researchers could consider repeated cross-sectional surveying, SfM on non-

vegetated banks, or comparing successive DEMs made from LiDAR data (Jugie et al., 2018; Hamshaw et al., 2019; Chassiot et al., 2020).

There are also limitations in how critical shear stress values were calculated from statistical relationships that may not accurately represent the riverbank material. This study used a relationship that was developed for soils with similar grain size distributions, moisture content, and organic matter content to the study soils, but the silt-clay content for the study soils was higher than the soils for which the relationship was developed (Julian and Torres, 2006). Also, this method only considers one soil property, even though a combination of unique properties impact soil strength (Mahalder et al., 2018). In future studies, direct measurement techniques, such as jet tests, are recommended to improve the accuracy of critical shear stress estimates (Hanson and Cook, 2004).

More limitations involve making a realistic hydraulic model which may cause modeled shear stress values to not be representative of the study sites. Bank stability was assumed to be spatial constant, rather than varying as it could in a bank model such as BSTEM using RipRoot (Stryker et al., 2017; Stover et al., 2018). In addition, bank erosion estimates focused on the mechanism of fluvial entrainment, though other important erosive processes such as mass failure and subaerial weakening were likely present at study sites (Klavon et al., 2017; Stryker et al., 2017; Stover et al., 2018). Further efforts to quantify additional erosional processes could improve the explanatory ability of model estimates. This could potentially be done using other models, such as RipRoot combined with BSTEM, which take into account bank material and the effect of root density and strength on the stability of the bank material (Stryker et al., 2017;

Stover et al., 2018). Understanding what mechanisms of erosion are influenced by knotweed can help determine how to better protect against its effects.

One difficulty in producing the model, especially at higher discharges, was the inability to obtain enough accurate stage measurements during high flow conditions to set up and validate the model. This study used WSE values from the day the reach was surveyed to validate the model at low-flow conditions, resulting in quite good agreement during low flows. At larger flows, which covered more of and even exceeded the bankfull channel, no validation data were available, so the accuracy of the model under those conditions cannot be quantified. Model inputs, including discharge, downstream stage, and upstream stage, were estimated for each reach as best as possible, but still add potential error to the analysis. Discharge was estimated using the percentage of the watershed draining to the reach multiplied by the discharge at the gauging station, but other methods could be used including measuring discharge directly at the site. River stage at each site could also be monitored through the use of a pressure transducer and used to develop a stage-discharge relationship for each site. Similar studies in the future should attempt to minimize potential sources of error around discharge and water surface elevation measurements in order to create accurate hydraulic models.

5.3 Recommendations for River Management

As the frequency of large erosion-causing floods is expected to increase in the future throughout New England (Armstrong et al., 2012; Armstrong et al., 2014; Ross et al., 2019), it is important as ever for river management to consider riverbank erosion and its implications. Riverbank erosion can cause loss of property and damage to infrastructure as well as harmful impacts to fluvial ecosystems by increasing suspended sediment and contaminants within the

river (Gall et al., 2011, Fluixá-Sanmartín et al., 2018; Deng et al., 2016; Ross et al., 2019; Li et al., 2021).

In some cases, dams, levees, embankments, and bank revetment can be used to control river flow and stabilize banks to minimize damages due to high discharges. These structures can be expensive to employ and may negatively impact erosion and depositional patterns in rivers (Gilvear and Winterbottom, 1992). In some cases, these structures can cause more erosion and in others, specifically upstream of dams and levees, can cause deposition of sediment (Gilvear and Winterbottom, 1992). In addition, dams and bank revetment have failed in large floods endangering lives and causing costly damage (Gilvear and Winterbottom, 1992).

River management should consider taking preventative measures against bank erosion before bank revetment is necessary. This study found riverbanks with Itadori knotweed experienced more erosion on average than riverbanks with native vegetation, which agrees with past studies (Mummigatti, 2008; Secor et al. 2013; Arnold and Toran, 2018; Hammer, 2019; Matte et al., 2021). To minimize the impacts on river ecosystems by knotweed, river corridor management should consider efforts to remove knotweed from river systems before the need for expensive revetment (Colleran et al., 2020). As knotweed is highly invasive and can be difficult to remove, ideally removal efforts should be started while there are minimal knotweed patches within a river system (Colleran and Goodall, 2014; Colleran and Goodall, 2015; Colleran et al., 2020; Drazan et al., 2021). If removal along an entire river system is not an option, river management could work to prevent the spread of knotweed by informing property owners of its invasive nature and give information about how to remove it themselves.

In summary, the results of this study suggest that knotweed may increase erosion rates of riverbanks which can negatively impact fluvial ecosystems and cause costly damage to

infrastructure (Gall et al., 2011; Arnold and Toran, 2018; Fluixá-Sanmartín et al., 2018; Deng et al., 2016; Ross et al., 2019; Li et al., 2021). As such, the implications of knotweed on riverbank erosion warrants consideration by river corridor management.

REFERENCES

Arcement, G.J., Schneider, V.R. (1989). Guide for selecting manning's roughness coefficients for natural channels and flood plains.

Armstrong, W.H., Collins, M.J., Snyder, N.P. (2012). Increased frequency of low-magnitude floods in New England, Journal of the American Water Resources Association, 48(2), 306-320.

Armstrong, W. H., Collins, M.J., Snyder, N.P. (2014). Hydroclimatic flood trends in the northeastern United States and linkages with large-scale atmospheric circulation patterns, Hydrological Sciences Journal, 59(9), 1636-1655.

Arnold, E., Toran, L. (2018). Effects of bank vegetation and incision on erosion rates in an urban stream, Water, 10(4), 482.

Bangen, S. G., Wheaton, J. M., Bouwes, N., Bouwes, B., Jordan, C. (2014). A methodological intercomparison of topographic survey techniques for characterizing wadeable streams and Rivers, Geomorphology, 206, 343–361. https://doi.org/10.1016/j.geomorph.2013.10.010

Brater, E.F., King, H.W. (1982). Handbook of hydraulics for the solution of hydraulic engineering problems (6th ed.), Mcgraw-Hill Book Company.

Bywater-Reyes, S., Diehl, R.M., Wilcox, A.C. (2018). The influence of a vegetated bar on channel-bend flow dynamics, Earth Surface Dynamics, 6(2), 487-503.

Chassiot, L., Lajeunesse, P., Bernier, J. (2020). Riverbank erosion in cold environments: Review and outlook, Earth-Science Reviews, 207.

Child, L. E., Wade, M. (2000). The Japanese knotweed manual. Chichester, UK: Packard Publishing Limited, Volume 1, 123p.

Clapuyt, F., Vanacker, V., Van Oost, K. (2016). Reproducibility of UAV-based earth topography reconstructions based on Structure-from-Motion algorithms, Geomorphology, 260, 4–15. https://doi.org/10.1016/j.geomorph.2015.05.011

Colleran, B. P., Goodall, K. E. (2014). In Situ Growth and Rapid Response Management of Flood-Dispersed Japanese Knotweed (Fallopia japonica), Invasive Plant Science and Management, 7(1), 84–92. Https://doi.org/10.1614/ipsm-d-13-00027.1

Colleran, B. P., Goodall, K. E. (2015). Extending the Timeframe for Rapid Response and Best Management Practices of Flood-Dispersed Japanese Knotweed (Fallopia japonica), Invasive Plant Science and Management, 8(2), 250–253. Https://doi.org/10.1614/ipsm-d-14-00046.1

Colleran, B., Lacy, S. N., Retamal, M. R. (2020). Invasive Japanese knotweed (Reynoutria japonica Houtt.) and related knotweeds as catalysts for streambank erosion, River Research and Applications, 36(9), 1962-1969.

Coulthard, T. J. (2005). Effects of vegetation on braided stream pattern and dynamics, Water Resources Research, 41(4). Https://doi.org/10.1029/2004wr003201

Couper, P., Stott, T., Maddock, I. (2002). Insights into riverbank erosion processes derived from analysis of negative erosion-pin recordings: observations from three recent UK studies, Earth Surface Processes and Landforms, 27(1), 59–79. Https://doi.org/10.1002/esp.285

Deng, L., Wang, W., Yu, Y. (2016). State-of-the-art review on the causes and mechanisms of bridge collapse, Journal of Performance of Constructed Facilities, 30(2). https://doi.org/10.1061/(asce)cf.1943-5509.0000731

Drazan, D., Smith, A. G., Anderson, N. O., Becker, R., Clark, M. (2021). History of knotweed (Fallopia spp.) Invasiveness, Weed Science, 69(6), 617–623. https://doi.org/10.1017/wsc.2021.62

Duquette, M. C., Compérot, A., Hayes, L. F., Pagola, C., Belzile, F., Dubé, J., Lavoie, C. (2016). From the source to the outlet: Understanding the distribution of invasive knotweeds along a North American River, River Research and Applications, 32(5), 958–966. https://doi.org/10.1002/rra.2914

Duró, G., Crosato, A., Kleinhans, M. G., Winkels, T. G., Woolderink, H. A. G., Uijttewaal, W. S. J. (2019). Distinct patterns of bank erosion in a navigable regulated river, Earth Surface Processes and Landforms, 45(2), 361–374. https://doi.org/10.1002/esp.4736

Fluixà-Sanmartín, J., Altarejos-García, L., Morales-Torres, A., Escuder-Bueno, I., 2018. Climate change impacts on dam safety, Natural Hazards and Earth System Sciences, 18(9), 2471-2488.

Fogelman, J.K., Bilger, M.D., Holt, J.R., Matlaga, D.P. (2018). Decomposition and benthic macroinvertebrate communities of exotic Japanese knotweed (Fallopia japonica) and American sycamore (Platanus occidentalus) detritus within the Susquehanna River, Journal of Freshwater Ecology, 33:1, 299-310, DOI: 10.1080/02705060.2018.1458660

Foucher, A., Salvador-Blanes, S., Vandromme, R., Cerdan, O., Desmet. (2016). Quantification of bank erosion in a drained agricultural lowland catchment, Hydrological Processes. 31. 10.1002/hyp.11117.

Gall, M., Borden, K. A., Emrich, C. T., Cutter, S. L. (2011). The unsustainable trend of natural hazard losses in the United States, Sustainability, 3(11), 2157 – 2181. https://doi.org/10.3390/su3112157

Galster, J. C. (2007). Natural and anthropogenic influences on the scaling of discharge with drainage area for multiple watersheds, Geosphere, 3(4), 260. https://doi.org/10.1130/ges00065.1

Gasser, E., Perona, P., Dorren, L., Phillips, C., Hübl, J., Schwarz, M. (2020). A New Framework to Model Hydraulic Bank Erosion Considering the Effects of Roots. Water, 12(3), 893. MDPI AG. Retrieved from http://dx.doi.org/10.3390/w12030893

Gilvear, D. J. Winterbottom, S. J. (1992). Channel change and flood events since 1783 on the regulated River Tay, Scotland: implications for flood hazard management, Regulated Rivers 7, 247-260.

Gran, K.B., Paola, C. (2001). Riparian vegetation controls on braided stream dynamics, Water Resources Research, 37, 3275 - 3283.

Gurnell, A.M., Corenblit, D., García de Jalón, D., González del Tánago, M., Grabowski, R.C., o'hare, M. T., Szewczyk, M. (2016). A conceptual model of vegetation–hydrogeomorphology interactions within river corridors, River research and applications, 32(2), 142-163.

Hammer, C. F. (2019). The impacts of terrestrial invasive plants on streams and natural and restored riparian forests in Northern New England. A master's thesis in pursuit of a Forestry degree from the University of New Hampshire.

Hamshaw, S. D., Engel, T., Rizzo, D., O'Neil-Dunne, J., Dewoolkar, M.M. (2019) Application of unmanned aircraft systems for streambank erosion monitoring along river corridors, Geomatics, Natural Hazards, Risk. Doi.org/10.1080/19475705.2019.1571533

Hanson, G. J. (1990). Surface erodibility of earthen channels at high stresses part II – developing an in-situ testing device, Transactions of the ASAE 33(1): 132−137.

Hanson, G.J., Cook, K. (2004). Apparatus, test procedures, and analytical methods to measure soil erodibility in situ, Applied Engineering in Agriculture, 20, 455-462.

Hemmelder, S., Marra, W., Markies, H., De Jong, S. (2018). Monitoring river morphology & bank erosion using UAV imagery – A case study of the river Buëch, Hautes-Alpes, France, International Journal of Applied Earth Observation and Geoinformation. 73. 428-437. 10.1016/j.jag.2018.07.016.

Heritage, G. L., Milan, D. J., Large, A. R. G., Fuller, I. C. (2009). Influence of survey strategy and interpolation model on DEM quality, Geomorphology, 112(3-4), 334–344. Https://doi.org/10.1016/j.geomorph.2009.06.024

Jugie, M., Gob, F., Virmoux, C., Brunstein, D., Tamisier, V., Lecoeur, C., Grancher, D. (2018). Characterizing and Quantifying the Discontinuous Bank Erosion of a Small Low Energy River Using Structure-from-Motion Photogrammetry and Erosion Pins, Journal of Hydrology. 563. 10.1016/j.jhydrol.2018.06.019.

Julian, J.P., Torres, R. (2006). Hydraulic erosion of cohesive riverbanks, Geomorphology, 76, 193-206.

Klavon, K., Fox, G., Guertault, L., Langendoen, E., Enlow, H., Miller, R., Khanal, A. (2017). Evaluating a process-based model for use in streambank stabilization: Insights on the Bank Stability and Toe Erosion Model (BSTEM), Earth Surface Processes.

Kline, M., Dolan, K., (2008). Vermont Agency of Natural Resources river corridor protection guide: Fluvial geomorphic-based methodology to reduce flood hazards and protect water quality.

Langendoen, E. J. (2000). CONCEPTS—Conservational Channel Evolution and Pollutant Transport System, Res. Rep. 16, Natl. Sediment. Lab., U.S. Dep. Of Agric., Oxford, Miss.

Lavoie, C. (2017). The impact of invasive knotweed species (Reynoutria spp.) on the environment: Review and research perspectives, Biological Invasions, 19(8), 2319–2337. Https://doi.org/10.1007/s10530-017- 1444-y

Lawler, D. (1993). The measurement of river bank erosion and lateral channel change: A review, Earth Surface Processes and Landforms, 18, 777-821.

Lawler, D. (1995). The Impact of Scale on the Processes of Channel-Side Sediment Supply: A Conceptual Model. Effects of Scale on Interpretation and Management of Sediment and Water Quality. 226.

Lawler, D.M., Leeks, G.J. (1992) River bank erosion events on the Upper Severn detected by the Photo-Electronic Erosion Pin (PEEP) system. Erosion and Sediment Transport Monitoring Programs in River Basins (Proceedings of the Oslo Symposium, August 1992). IAHS Publ. no. 210.

Li, X., Cooper, J. R., Plater, A. J. (2021). Quantifying erosion hazards and economic damage to critical infrastructure in river catchments: Impact of a warming climate, Climate Risk Management, 32, 100287. https://doi.org/10.1016/j.crm.2021.100287

Mahalder, B., Schwartz, J., Palomino, A., Zirkle, J. (2018). Estimating Erodibility Parameters for Streambanks with Cohesive Soils Using the Mini Jet Test Device: A Comparison of Field and Computational Methods, Water, 10(3), 304. Https://doi.org/10.3390/w10030304

Martin, F. M., Müllerová, J., Borgniet, L., Dommanget, F., Breton, V., Evette, A. (2018). Using single- and multi-date UAV and satellite imagery to accurately monitor invasive knotweed species. Remote Sensing, 10(10), 1662. Https://doi.org/10.3390/rs10101662

Matte, R., Boivin, M., Lavoie, C. (2021). Japanese knotweed increases soil erosion on riverbanks, River Research and Applications, 38(3), 561–572. Https://doi.org/10.1002/rra.3918

Matthes, W. J., Sholar, C. J., George, J. R. (1992). Quality-assurance plan for the analysis of fluvial sediment by laboratories of the U.S. Geological Survey. Open-File Report. Https://doi.org/10.3133/ofr91467

Mummigatti, K. (2008). The effects of Japanese Knotweed (Reynoutria japonica) on riparian lands in Otsego County, New York.

Nardi, L., Campo, L., Rinaldi, M. (2013). Quantification of riverbank erosion and application in risk analysis, Natural hazards, 69(1), 869-887.

Nelson, J. M. (2013). iRIC Software: Fastmech solver manual. USGS, 1–36.

Palace, M., Herrick, C., DelGreco, J., Finnell, D., Garnello, A., McCalley, C., McArthur, K., Sullivan, F., Varner, R. (2018). Determining Subarctic Peatland Vegetation Using an Unmanned Aerial System (UAS), Remote Sensing, 10(9), 1498. https://doi.org/10.3390/rs10091498

Perignon, M. C., Tucker, G. E., Griffin, E. R., Friedman, J. M. (2013). Effects of riparian vegetation on topographic change during a large flood event, Rio Puerco, New Mexico, USA, Journal of Geophysical Research: Earth Surface, 118(3), 1193-1209.

Pollen, N., Simon, A. (2005). Estimating the mechanical effects of riparian vegetation on stream bank stability using a fiber bundle model, Water Resources Research, 41(7). https://doi.org/10.1029/2004wr003801

Rinaldi, M., Mengoni, B., Luppi, L., Darby, S.E., Mosselman, E. (2008). Numerical simulation of hydrodynamics and bank erosion in a river bend, Water Resources Research, 44.

Ross, D. S., Wemple, B. C., Willson, L. J., Balling, C. M., Underwood, K. L., Hamshaw, S. D. (2019). Impact of an extreme storm event on river corridor bank erosion and phosphorus mobilization in a mountainous watershed in the Northeastern United States, Journal of Geophysical Research: Biogeosciences, 124, 18–32. https://doi.org/10.1029/2018JG004497

Secor, E., Ross, D., Balling, C. (2013). Japanese knotweed effects on erosion rates in riparian corridors.

Shannon, C.E. (1948). A mathematical theory of communication. Bell System Technical Journal: 27, 379–423. https://doi.org/10.1002/j.1538-7305.1948.tb01338.x

Simon, A., Collison, A.J. (2002). Quantifying the mechanical and hydrologic effects of riparian vegetation on streambank stability, Earth Surface Processes and Landforms, 27.

Simon, A., Collison, A.J., Layzell, A.L. (2003). Incorporating Bank-Toe Erosion by Hydraulic Shear into the ARS Bank- Stability Model: Missouri River, Eastern Montana.

Smets, T., Poesen, J., Bochet, E. (2008). Impact of plot length on the effectiveness of different soil-surface covers in reducing runoff and soil loss by water, Progress in Physical Geography, 32(6), 654–677. https://doi.org/10.1177/0309133308101473

Web Soil Survey. Natural Resources Conservation Service, United States Department of Agriculture. Available online at the following link: http://websoilsurvey.sc.egov.usda.gov/. Accessed [9/14/2022].

Stover, J. E., Keller, E. A., Dudley, T. L., Langendoen, E. J. (2018). Fluvial geomorphology, root distribution, and tensile strength of the invasive giant reed, Arundo donax and its role on stream bank stability in the Santa Clara River, Southern California, Geosciences, 8(8), 304.

Streamstats: Streamflow Statistics and Spatial Analysis Tools for Water-Resources Applications, https://www.usgs.gov/mission-areas/water-resources/science/streamstats-streamflowstatistics-and-spatial-analysis-tools.

Stryker, J., Wemple, B., Bomblies, A. (2017). Modeling sediment mobilization using a distributed hydrological model coupled with a bank stability model, Water Resources Research, 53(3), 2051-2073.

Talmage, E., Kiviat, E. (2004), Japanese knotweed and water quality on the Batavia Kill in Greene County, New York: Background information and literature review Rep., Report to the Greene County Soil and Water Conservation District and the New York City Department of Environmental Protection. Hudsonia Ltd., Annandale, NY

Tanner, P. A., Leong, L. S. (1995). The effects of different drying methods for marine sediment upon moisture content and metal determination, Marine Pollution Bulletin, 31(4-12), 325–329. Https://doi.org/10.1016/0025-326x(95)00172-j

Thorne, C.R. (1990). Effects of vegetation on river bank erosion and stability.

Thorne, C.R., (1982). Processes and mechanisms of river bank erosion. In: Hey, R.D., Bathurst, J.C., Thorne, C.R. (Eds.), Gravel-Bed Rivers. Wiley, Chichester, pp. 227–259.

USGS NWIS, USGS 01073500 Lamprey River near Newmarket, NH, https://waterdata.usgs.gov/monitoring-location/01073500.

USGS NWIS, USGS 01152500 Sugar River at West Claremont, NH https://waterdata.usgs.gov/monitoring-location/01152500.

USGS waterwatch (n.d.) Waterwatch.usgs.gov. Retrieved December 22, 2022, from https://waterwatch.usgs.gov/

Van Oorschot, M., Kleinhans, M. G., Geerling, G. W., Egger, G., Leuven, R. S. E. W., Middelkoop, H. (2017). Modeling invasive alien plant species in river systems: Interaction with native ecosystem engineers and effects on hydro-morphodynamic processes, Water Resources Research, 53(8), 6945–6969. Https://doi.org/10.1002/2017WR02 0854

Wahl, T.L. (2016). The submerged jet erosion test: past-present-future.

Wigmosta, M.S., Vail, L.W., Lettenmaier, D.P. (1994). A distributed hydrology-vegetation model for complex terrain, Water Resources Research, 30, 1665-1679.

Wilson, M. J., Freundlich, A. E., Martine, C. T. (2017). Understory dominance and the new climax: Impacts of Japanese knotweed (Fallopia japonica) invasion on native plant diversity and recruitment in a riparian woodland, Biodiversity data journal, (5), e20577. Https://doi.org/10.3897/BDJ.5.e20577

APPENDIX

Table 10. Raw bank pin data

Bank Pin	8/11/2021	8/18/2021	9/23/2021	10/14/2021	12/10/2021	4/29/2022	9/30/2022	Total*
Sugar 1								
S11T N							-0.6	-0.6
S11M N							1	1
S11B N							-0.3	-0.3
S12T N							-6.3	-6.3
S12M N							-2	-2
S12B N							-5.2	-5.2
S13T KW							-4	-4
S13M KW							-22.3	-22.3
S13B KW							-19.6	-19.6
S14T KW							-11.5	-11.5
S14M KW							-19.5	-19.5
S14B KW							-26.2	-26.2
Sugar 2								
S21T N				0.2	-0.4	-1.6	-1.9	-1.9
S21M N				-0.3	-0.4	-8.4	-8.5	-8.5
S21B N				0.4	0.7	-0.7	6.6	6.6
S22T N				0	-0.2	-2.3	2.7	2.7
S22M N				-0.3	-0.4	-11.2	-8.8	-16.7
S22B N				0.6	0.8	-7.7	-6	-6
S23T KW				0.4	0.5	-1.5	-0.7	-0.7
S23M KW				0.5	-0.3	-7.9	-2.8	-8.3
S23B KW				0.1	-1.1	-9.2	-0.8	-9.9
S24T KW				-0.2	-0.5	-19.6	-14.8	-19.6
S24M KW				0.3	0.2	-4.4	-1	-4.7
S24B KW				0.4	0.3	-7	0.6	-6

* Total erosion and deposition including pin reset measurements.
NR = Not recovered
UW = Under Water and unable to be measured

Table 10. (continued)

Bank Pin	8/11/2021	8/18/2021	9/23/2021	10/14/2021	12/10/2021	4/29/2022	9/30/2022	Total*
Sugar 3								
S31T KW							-3.6	-3.6
S31M KW							-18.1	-18.1
S31B KW							-4.7	-4.7
S32T KW							-1.8	-1.8
S32M KW							-20.8	-20.8
S32B KW							-4.3	-4.3
S33T N								NR
S33M N								NR
S33B N								NR
S34T N								NR
S34M N								NR
S34B N								NR
Sugar 4								
S41T N							-10.7	-10.7
S41M N							-7.5	-7.5
S41B N							-1.6	-1.6
S42T N							-3.6	-3.6
S42M N							-1.9	-1.9
S42B N							-2.7	-2.7
S43T KW							-7.2	-7.2
S43M KW							1	1
S43B KW							-37.3	-37.3
S44T KW							-13.4	-13.4
S44M KW							-18.9	-18.9
S44B KW							-21.2	-21.2

* Total erosion and deposition including pin reset measurements.
NR = Not recovered
UW = Under Water and unable to be measured

Table 10. (continued)

Bank Pin	8/11/2021	8/18/2021	9/23/2021	10/14/2021	12/10/2021	4/29/2022	9/30/2022	Total*
Sugar 5								
S51T N							NR	
S51M N							NR	
S51B N							-7.6	-7.6
S52T N							3.6	3.6
S52M N							-0.9	-0.9
S52B N							-4.7	-4.7
S53T KW							0.4	0.4
S53M KW							-4.7	-4.7
S53B KW							-7.7	-7.7
S54T KW							-0.1	-0.1
S54M KW							-5.6	-5.6
S54B KW							-2.7	-2.7
Sugar 6								
S61T N			-0.3		-2.9	-33.4	2.7	-33.2
S61M N			0		-11.7	NR	NR	-17.1
S61B N			-0.9		UW	-4.2	-19.1	-19.1
S62T N			-0.1		-0.1	NR	NR	NR
S62M N			-0.3		-4	-4.1	NR	NR
S62B N			-0.2		UW	NR	NR	NR
S63T KW			-0.1		-1.9	-20.5	-7.2	-21.5
S63M KW			-0.5		-5.6	-6.2	-13.5	-22.6
S63B KW			-0.6		UW	-4.4	-21.8	-21.8
S64T KW			-0.6		-3.8	-23.5	1.6	-18.4
S64M KW			0.1		0.2	-3.4	-1.2	-8.6
S64B KW			-0.2		UW	-0.5	-14.2	-14.2
Lamprey 1								
L1T KW					-1	-2	11.9	-2.4
L1M KW					-1.1	-3.8	12.4	-4.2
L1B KW					-0.9	-7.6	21.9	-10.9
L2T KW					0.2	0.3	7.8	0
L2M KW					0.1	-10.4	21.2	-15.4
L2B KW					-2.7	3.9	11.7	-3.8
L3T N					1.7	1.4	7.2	1.3
L3M N					2.8	9.3	1.6	7.7
L3B N					8.5	1.4	7.3	1.2
L4T N					0.1	-0.3	7.8	-0.3
L4M N					0.2	5	4.9	0.1
L4B N					2.8	0.2	10.1	0.1

* Total erosion and deposition including pin reset measurements.
NR = Not recovered
UW = Under Water and unable to be measured